

Energy-conserving finite difference scheme based on velocity interpolation applicable to unsteady flows using collocated grids

Hideki Yanaoka *

Department of Systems Innovation Engineering,
Faculty of Science and Engineering, Iwate University,
4-3-5 Ueda, Morioka, Iwate 020-8551, Japan

October 13, 2023

ABSTRACT

The collocation method uses the Rhie–Chow scheme to find the cell interface velocity by pressure-weighted interpolation. The accuracy of this interpolation method in unsteady flows has not been fully clarified. This study constructs a finite difference scheme for incompressible fluids using a collocated grid in a general curvilinear coordinate system. The velocity at the cell interface is determined by weighted interpolation based on the pressure difference to prevent pressure oscillations. The Poisson equation for the pressure correction value is solved with the cross-derivative term omitted to improve calculation efficiency. In addition, simultaneous relaxation of velocity and pressure is applied to improve convergence. Even without the cross-derivative term, calculations can be stably performed, and convergent solutions are obtained. In unsteady inviscid flow, the conservation of kinetic energy is excellent even in a non-orthogonal grid, and the calculation result has second-order accuracy to time. In viscous analysis at a high Reynolds number, the error decreases compared with that of the Rhie–Chow interpolation method. The present numerical scheme improves calculation accuracy in unsteady flows. The possibility of applying this computational method to high Reynolds number flows is demonstrated through several analyses.

Keywords Collocated grid, Kinetic energy conservation, Interpolation, Simultaneous relaxation, Incompressible flow, Finite difference method

1 Introduction

Numerical methods for incompressible flows usually use staggered grids to eliminate spurious errors for pressure. In this case, the calculation code becomes complicated because the definition points for each velocity component and pressure are different. For general curvilinear coordinate systems, it is hard to satisfy the conservation law discretely using staggered grids. In addition, it is not easy to set boundary conditions.

On the other hand, a method that does not use staggered grids has been proposed. Rhie and Chow (1983) eliminates pressure spurious errors by interpolating velocities with pressure gradient weights at cell interfaces. This method is called pressure interpolation or momentum interpolation. Later, Perić et al. (1988) and Majumdar (1988) improved the interpolation method. Zang et al. (1994) have extended the fractional-step method of Kim and Moin (1985) to general curvilinear coordinate systems using collocated grids. They adopted a method of interpolating the velocity by shifting upstream at the cell interface. The pressure interpolation of Rhie and Chow (1983) is known to have shortcomings. Improvement is necessary to obtain a convergent solution that does not depend on a time step (Choi, 1999), and when the time step is small, pressure spurious errors occur (Yu et al., 2002). Bartholomewa et al. (2018) proposed a unified and consistent formulation of Rhie–Chow’s momentum interpolation and analyzed incompressible and low Mach number flows. Lee et al. (2019) reported that the error of the continuity equation defined by the velocity at the cell center becomes second-order accuracy to time when interpolation by pressure difference is used. The numerical

*Email address for correspondence: yanaoka@iwate-u.ac.jp

method using a collocated grid affects the conservation of kinetic energy (Morinishi, 1998, 1999) even without using Rhie–Chow pressure interpolation. On the other hand, no studies refer to energy conservation when using pressure interpolation. The report of Lee et al. (2019) does not concretely show the energy conservation property. To the best of the author’s knowledge, the effect of interpolating the velocity at the cell interface on the time accuracy has not been investigated in the analysis of unsteady flows.

Numerical methods such as SIMPLE (Semi-Implicit Method for Pressure-Liked Equation) (Patankar and Spalding, 1972; Van Doormaal and Raithby, 1984) and MAC (Marker and Cell) (Harlow and Welch, 1965; Amsden and Harlow, 1970; Hirt et al., 1975) are used for analyzing incompressible flows. When the SIMPLE and MAC methods are expanded to general curvilinear coordinate systems, cross-derivative terms always appear in the fundamental equations. When the Poisson equation for pressure or pressure correction value is discretized by the central difference scheme with second-order accuracy, the coefficients of the Poisson equation with cross terms are 19 components. When analyzing a complicated three-dimensional flow field, the increase in memory usage and computation time results in inefficient computation. Therefore, it is necessary to construct a method that can perform stable and highly accurate calculations even if the cross terms are omitted. In particular, when solving the Poisson equation for pressure, the treatment method for the cross terms leads to computational instability. In numerical methods of the SIMPLE family, convergence and computational accuracy in the analysis without the cross terms have been investigated. Perić (1990) analyzed a two-dimensional cavity flow using a non-orthogonal grid system and found that omitting the cross term of the Poisson equation for the pressure correction value leads to slow convergence when using a highly strained grid. It is also revealed that in a distorted non-orthogonal grid system, the range of under-relaxation coefficient over which the calculation converges is very narrow. Wu et al. (1995) reported that the omission of the cross term in the Poisson equation leads to significant differences with existing values.

To analyze unsteady flows with high accuracy using collocated grids, we should investigate the effect of interpolating the velocity at the cell interface on the time accuracy. It is also necessary to consider an efficient method of solving pressure. From the above points of view, in this research, we construct a finite difference scheme for incompressible flows in a general curvilinear coordinate system using a collocated grid and investigate kinetic energy conservation properties and an efficient method of finding pressure. The outline of the present numerical method is as follows: The SMAC (Simplified Marker and Cell) method (Amsden and Harlow, 1970), which is a numerical method using staggered grids, is extended to collocated grid systems. We improve the pressure interpolation of Rhie and Chow (1983) so that the time discretization is the second-order accuracy in unsteady fields. In addition, we introduce the idea of HSMAC (Highly Simplified MAC) (Hirt et al., 1975) so that convergence does not deteriorate even if the cross terms are omitted. This method simultaneously relaxes the Poisson equation for the pressure correction value and the modified equations for velocity and pressure. Using the computational method proposed in this study, we analyze several flow fields and verify that the time discretization accuracy can be improved in unsteady flow fields.

The remainder of this paper is organized as follows: Section 2 presents the fundamental equations and mentions the transport equation for kinetic energy and the conservation property. In Section 3, the governing equations in the Cartesian coordinate system are transformed into the general curvilinear coordinate system so that flow fields with arbitrary-shaped boundaries can be analyzed. In Section 4, we investigate the accuracy of interpolating cell interface velocities and construct an improved method of Rhie–Chow’s interpolation method. Section 5 extends the interpolation method used in this study to general curvilinear coordinate systems and proposes a simultaneous relaxation method to solve the governing equations. Section 6 analyzes several flow models using this numerical method and investigates the kinetic energy conservation properties and computational accuracy. Finally, Section 7 presents a summary of the results.

2 Fundamental equations

This study deals with three-dimensional incompressible viscous flow and considers natural convection with small density change. The non-dimensionalized fundamental equations are the continuity equation, the Navier-Stokes equation under the Boussinesq approximation, and the energy equation, as follows:

$$\frac{\partial u_j}{\partial x_j} = 0, \quad (2.1)$$

$$\frac{\partial u_i}{\partial t} + \frac{\partial}{\partial x_j}(u_j u_i) = -\frac{\partial p}{\partial x_i} + \frac{1}{Re} \frac{\partial^2 u_i}{\partial x_j \partial x_j} - \frac{Ra}{Re^2 Pr} T e_i, \quad (2.2)$$

$$\frac{\partial T}{\partial t} + \frac{\partial}{\partial x_j}(u_j T) = \frac{1}{Re Pr} \frac{\partial^2 T}{\partial x_j \partial x_j}, \quad (2.3)$$

Nomenclature

e_i	unit vector in direction of gravity	ΔT	temperature difference, K
g	gravity acceleration, m/s ²	Δx_i	grid width, m
g_{mn}	metric tensor	λ	$\lambda = 1, 2$
J	Jacobian	μ	viscosity coefficient, Pa s
k	thermal conductivity, W/(m K)	ν	kinematic viscosity, m ² /s
K	kinetic energy, J/kg	ξ_m	coordinate in computational space
Nu	Nusselt number	ρ	density, kg/m ³
p	pressure, Pa	ϕ	pressure correction value
Pr	Prandtl number	<i>Subscript</i>	
Ra	Rayleigh number	i, j, k	coordinate direction identifiers, or grid points
t	time, s	m, n	coordinate direction identifiers
T	temperature, K	w	wall
u_i	flow velocity (u, v, w), m/s	ref	reference value
U_i	cell interface velocity, m/s	<i>Superscript</i>	
U_m	contravariant velocity	l	number of simultaneous relaxation
x_i	coordinate (x, y, z), m	m	Newton iterative level
<i>Greek symbols</i>		n	time level
α	thermal diffusivity coefficient, m ² /s	$*$	non-dimensional variable
β	volume expansion coefficient, 1/K	\wedge	predicted value
δ_1, δ_2	difference operator	$-$	interpolated value
Δt	time increment, s		

where $i, j = 1, 2, 3$ are the x -, y -, and z -components, respectively. t is the time, x_i is coordinate, u_i is the flow velocity, p is the pressure, T is the temperature, g is the acceleration of gravity, e_i is the unit vector in the direction of gravity. Re is the Reynolds number, Pr is the Prandtl number, and Ra is the Rayleigh number. As reference values used for non-dimensionalization, the length is l_{ref} , the velocity is u_{ref} , and the temperature is T_{ref} . The variables of the fundamental equations were non-dimensionalized by using these reference values as follows:

$$x_i^* = \frac{x_i}{l_{ref}}, \quad u_i^* = \frac{u_i}{u_{ref}}, \quad p^* = \frac{p}{\rho u_{ref}^2}, \quad t^* = \frac{u_{ref} t}{l_{ref}}, \quad T^* = \frac{T - T_{ref}}{\Delta T}, \quad \Delta T = T_w - T_{ref}, \quad (2.4)$$

where the superscript $*$ represents the non-dimensional variable, and the superscript $*$ was omitted in the fundamental equations. T_w is the temperature at the wall. The non-dimensional parameters in the fundamental equation are defined as

$$Re = \frac{u_{ref} l_{ref}}{\nu}, \quad Pr = \frac{\nu}{\alpha}, \quad Ra = \frac{g \beta \Delta T l_{ref}^3}{\nu \alpha}, \quad (2.5)$$

where ν is the kinematic viscosity of the fluid, α is the thermal diffusivity coefficient, and β is the volume expansion coefficient.

Kinetic energy is defined as $K = u_i u_i / 2$. For inviscid flow with $Re = \infty$, multiplying Eq. (2.2) by the velocity yields the following kinetic energy transport equation:

$$\frac{\partial K}{\partial t} + \frac{\partial}{\partial x_j} (u_j K) = - \frac{\partial u_i p}{\partial x_i} + p \frac{\partial u_i}{\partial x_i}. \quad (2.6)$$

From the continuity equation (2.1), the second term on the right-hand side becomes zero, and the above equation (2.6) is in conservative form. Therefore, kinetic energy is conserved in inviscid periodic flows. Depending on the discretization of the continuity equation (2.1) and the Navier–Stokes equation (2.2), the accuracy of the second term of Eq. (2.6) changes. Therefore, the discretization of the fundamental equation affects the conservation and calculation accuracy for kinetic energy.

3 Coordinate transformation

The fundamental equations in the Cartesian coordinate system are transformed into the general curvilinear coordinate system so that flow fields with arbitrary-shaped boundaries can be analyzed. The relationship between the

coordinates x_i in the physical space and the computational space ξ_m is given as follows:

$$x_i = x_i(\xi_1, \xi_2, \xi_3), \quad \xi_m = \xi_m(x_1, x_2, x_3). \quad (3.1)$$

By using the above relation, the fundamental equations are transformed into the general curvilinear coordinate system as follows:

$$\frac{1}{J} \frac{\partial JU_m}{\partial \xi_m} = 0, \quad (3.2)$$

$$\frac{\partial u_i}{\partial t} + \frac{1}{J} \frac{\partial}{\partial \xi_m} (JU_m u_i) = - \frac{\partial \xi_m}{\partial x_i} \frac{\partial p}{\partial \xi_m} + \frac{1}{Re} \frac{1}{J} \frac{\partial}{\partial \xi_m} \left(J g_{mn} \frac{\partial u_i}{\partial \xi_n} \right) - \frac{Ra}{Re^2 Pr} T e_i, \quad (3.3)$$

$$\frac{\partial T}{\partial t} + \frac{1}{J} \frac{\partial}{\partial \xi_m} (JU_m T) = \frac{1}{Re Pr} \frac{1}{J} \frac{\partial}{\partial \xi_m} \left(J g_{mn} \frac{\partial T}{\partial \xi_n} \right), \quad (3.4)$$

where J is the Jacobian, U_m is the contravariant velocity component, and g_{mn} is the metric tensor, which are defined by the following equations:

$$J = \det \left(\frac{\partial x_i}{\partial \xi_j} \right), \quad (3.5)$$

$$U_m = \frac{\partial \xi_m}{\partial x_j} u_j, \quad (3.6)$$

$$g_{mn} = \frac{\partial \xi_m}{\partial x_j} \frac{\partial \xi_n}{\partial x_j}. \quad (3.7)$$

det in the definition of the Jacobian J represents the determinant of the transformation matrix $[\partial x_i / \partial \xi_j]$. Each metric component $\partial \xi_m / \partial x_j$ and the Jacobian J are given as

$$\frac{\partial \xi_1}{\partial x_i} = \epsilon_{ijk} \frac{1}{J} \frac{\partial x_j}{\partial \xi_2} \frac{\partial x_k}{\partial \xi_3}, \quad \frac{\partial \xi_2}{\partial x_i} = \epsilon_{ijk} \frac{1}{J} \frac{\partial x_j}{\partial \xi_3} \frac{\partial x_k}{\partial \xi_1}, \quad \frac{\partial \xi_3}{\partial x_i} = \epsilon_{ijk} \frac{1}{J} \frac{\partial x_j}{\partial \xi_1} \frac{\partial x_k}{\partial \xi_2}, \quad (3.8)$$

$$J = \epsilon_{ijk} \frac{\partial x_i}{\partial \xi_1} \frac{\partial x_j}{\partial \xi_2} \frac{\partial x_k}{\partial \xi_3}, \quad (3.9)$$

where ϵ_{ijk} is the alternation symbol.

4 Weighted interpolation method for cell interface velocity

4.1 Definitions of finite difference and interpolation operations

The variables at a cell center (i, j, k) are defined as $\Phi_{i,j,k}$ and $\Psi_{i,j,k}$. The second-order central difference equation and interpolation for the variable Φ and the permanent product for two variables are as follows (Morinishi, 1998):

$$\left. \frac{\partial \Phi}{\partial x_1} \right|_{i,j,k} = \frac{\delta_1 \Phi}{\delta_1 x_1} = \frac{\bar{\Phi}_{i+1/2,j,k}^{x_1} - \bar{\Phi}_{i-1/2,j,k}^{x_1}}{\Delta x_1}, \quad (4.1)$$

$$\left. \frac{\partial \Phi}{\partial x_1} \right|_{i,j,k} = \frac{\delta_2 \Phi}{\delta_2 x_1} = \frac{\Phi_{i+1,j,k} - \Phi_{i-1,j,k}}{2\Delta x_1}, \quad (4.2)$$

$$\bar{\Phi}^{x_1} = \frac{\Phi_{i,j,k} + \Phi_{i+1,j,k}}{2}. \quad (4.3)$$

$$\widetilde{\Phi\Psi}^{x_1} \Big|_{i+1/2,j,k} = \frac{\Phi_{i,j,k} \Psi_{i+1,j,k} + \Phi_{i+1,j,k} \Psi_{i,j,k}}{2}, \quad (4.4)$$

where Δx_1 is the grid width in the physical space. The difference formula and interpolation for the x_2 - and x_3 -directions are similarly defined. The difference formula and interpolation in the case of coordinate transformation are similarly defined and given as

$$\left. \frac{1}{J} \frac{\partial J \xi_{1,1} \Phi}{\partial \xi_1} \right|_{i,j,k} = \frac{1}{J} \frac{(J \xi_{1,1} \bar{\Phi}^{\xi_1})_{i+1/2,j,k} - (J \xi_{1,1} \bar{\Phi}^{\xi_1})_{i-1/2,j,k}}{\Delta \xi_1}, \quad (4.5)$$

$$\bar{\Phi}^{\xi_1} \Big|_{i+1/2,j,k} = \frac{\Phi_{i,j,k} + \Phi_{i+1,j,k}}{2}, \quad (4.6)$$

where $\Delta\xi_1$ is the grid width in the computational space. The difference formula and interpolation for the ξ_2 - and ξ_3 -directions are similarly defined. The Jacobian is defined at cell centers.

If a variable at time level n is defined as Φ^n , the derivative and interpolation for the variable in time direction are similarly given as

$$\left. \frac{\partial \Phi}{\partial t} \right|^{n+1/2} = \frac{\Phi^{n+1} - \Phi^n}{\Delta t}, \quad (4.7)$$

$$\Phi^{n+1/2} = \frac{\Phi^{n+1} + \Phi^n}{2}, \quad (4.8)$$

where Δt is a time increment.

4.2 Interpolation of cell interface velocity

We explain the accuracy of Rhie–Chow pressure interpolation (Rhie and Chow, 1983) for unsteady analysis. We will use the fundamental equations without buoyancy force in the Cartesian coordinate system to briefly explain the interpolation method. The derivation of the following equations is the same, even using the coordinate-transformed governing equations. Regarding the discretization of the continuity equation (2.1) and the Navier–Stokes equation (2.2), we apply the implicit midpoint rule for the time derivative and the second-order central difference scheme for the spatial derivative. The discretized equation is given as

$$\frac{\delta_2 u_i^{n+1,m+1}}{\delta_2 x_i} = 0, \quad (4.9)$$

$$\frac{\delta_1 U_i^{n+1,m+1}}{\delta_1 x_i} = 0, \quad (4.10)$$

$$\frac{u_i^{n+1,m+1} - u_i^n}{\Delta t} = H_i^{n+\lambda,m+1} - \frac{\delta_2 p^{n+\lambda,m+1}}{\delta_2 x_i}, \quad (4.11)$$

$$H_i^{n+\lambda,m+1} = -\frac{\delta_1 U_j^{n+\lambda,m+1} \overline{u_i^{n+\lambda,m+1}}^{x_j}}{\delta_1 x_j} + \frac{1}{Re} \frac{\delta_1}{\delta_1 x_j} \left(\frac{\delta_1 u_i^{n+\lambda,m+1}}{\delta_1 x_j} \right), \quad (4.12)$$

$$u_i^{n+\lambda,m+1} = \lambda u_i^{n+1,m+1} + (1-\lambda) u_i^n, \quad (4.13)$$

$$U_i^{n+\lambda,m+1} = \lambda U_i^{n+1,m+1} + (1-\lambda) U_i^n, \quad (4.14)$$

$$p^{n+\lambda,m+1} = \lambda p^{n+1,m+1} + (1-\lambda) p^n, \quad (4.15)$$

where U_i represents the velocity at the cell interface. The superscripts n and m indicate the time and Newton iterative levels, respectively. The Newton method was applied to Eqs. (4.9), (4.10) and (4.11) to solve unsteady solutions. Regarding the discretization of the time derivative, if $\lambda = 1$, the Euler implicit method is applied to the time derivative. If $\lambda = 1/2$, the implicit midpoint rule is applied.

Applying the simplified marker and cell (SMAC) method (Amsden and Harlow, 1970), Eq. (4.11) is temporally split as follows:

$$\frac{\hat{u}_i^{n+1,m+1} - u_i^n}{\Delta t} = H_i^{n+\lambda,m+1} - \frac{\delta_2 p^{n+\lambda,m}}{\delta_2 x_i}, \quad (4.16)$$

$$\frac{u_i^{n+1,m+1} - \hat{u}_i^{n+1,m+1}}{\Delta t} = -\lambda \frac{\delta_2 \phi^m}{\delta_2 x_i}, \quad (4.17)$$

$$p^{n+1,m+1} = p^{n+1,m} + \phi^m, \quad (4.18)$$

where $\hat{u}_i^{n+1,m+1}$ is the predicted value of velocity, and ϕ^m is the pressure correction value. The velocity in $H_i^{n+1,m+1}$ is defined as $u_i^{n+\lambda} = \lambda \hat{u}_i^{n+1} + (1-\lambda) u_i^n$. Taking the divergence of Eq. (4.17) and using the continuity equation (4.9) at the $n+1$ level, the Poisson equation for the pressure correction value ϕ^m is derived as

$$\lambda \frac{\delta_2}{\delta_2 x_i} \left(\frac{\delta_2 \phi^m}{\delta_2 x_i} \right) = \frac{1}{\Delta t} \frac{\delta_2 \hat{u}_i^{n+1,m+1}}{\delta_2 x_i}. \quad (4.19)$$

In existing studies (Rhie and Chow, 1983; Perić et al., 1988; Majumdar, 1988; Zang et al., 1994; Morinishi, 1998; Choi, 1999; Morinishi, 1999; Yu et al., 2002; Bartholomewa et al., 2018; Lee et al., 2019), the formula (4.19) was not

used to obtain pressure or pressure correction value. The equation for modifying the velocity U_i at the cell interface is given as

$$\frac{U_i^{n+1,m+1} - \hat{U}_i^{n+1,m+1}}{\Delta t} = -\lambda \frac{\delta_1 \phi^m}{\delta_1 x_i}. \quad (4.20)$$

Taking the divergence of Eq. (4.20) and using the continuity equation (4.10) at the $n+1$ level, the Poisson equation for the pressure correction value ϕ^m is derived as

$$\lambda \frac{\delta_1}{\delta_1 x} \left(\frac{\delta_1 \phi^m}{\delta_1 x_i} \right) = \frac{1}{\Delta t} \frac{\delta_1 \hat{U}_i^{n+1,m+1}}{\delta_1 x_i}. \quad (4.21)$$

Generally, Eq. (4.21) is used to solve the pressure or pressure correction value. Using the velocity $\hat{u}_i^{n+1,m+1}$ at the cell center, the velocity $\hat{U}_i^{n+1,m+1}$ at the cell interface is obtained by direct interpolation as follows:

$$\hat{U}_i^{n+1,m+1} = \overline{\hat{u}_i^{n+1,m+1}}^{x_i}. \quad (4.22)$$

The continuity equation $\delta_2 u_i / \delta_2 x_i$ determined by the velocity at the cell center affects kinetic energy. Therefore, similar to existing research (Morinishi, 1999), we evaluate the error of the continuity formula. Using Eqs. (4.17) and (4.20), the continuity equation is given as

$$\begin{aligned} \frac{\delta_2 u_i^{n+1,m+1}}{\delta_2 x_i} &= \frac{\delta_1 \overline{u_i^{n+1,m+1}}^{x_i}}{\delta_1 x_i} = \frac{\delta_1}{\delta_1 x_i} \left(\overline{\hat{u}_i^{n+1,m+1}}^{x_i} - \Delta t \lambda \frac{\overline{\delta_2 \phi^m}^{x_i}}{\delta_2 x_i} \right) \\ &= \frac{\delta_1}{\delta_1 x_i} \left(U_i^{n+1,m+1} + \Delta t \lambda \frac{\delta_1 \phi^m}{\delta_1 x_i} - \Delta t \lambda \frac{\overline{\delta_2 \phi^m}^{x_i}}{\delta_2 x_i} \right) \\ &= \frac{\delta_1 U_i^{n+1,m+1}}{\delta_1 x_i} + \Delta t \lambda \frac{\delta_1}{\delta_1 x_i} \left(\frac{\delta_1 \phi^m}{\delta_1 x_i} - \frac{\overline{\delta_2 \phi^m}^{x_i}}{\delta_2 x_i} \right). \end{aligned} \quad (4.23)$$

If the continuity equation $\delta_1 U_i / \delta_1 x_i = 0$ obtained using the cell interface velocities is satisfied discretely, then the first term in the formula (4.23) can be ignored. Expanding the discrete value of the pressure correction value into a Taylor series, we can evaluate the error of the formula (4.23) as follows:

$$\frac{\delta_2 u_i^{n+1,m+1}}{\delta_2 x_i} = \Delta t \frac{\delta_1}{\delta_1 x_i} \left(\frac{\delta_1 \phi^m}{\delta_1 x_i} - \frac{\overline{\delta_2 \phi^m}^{x_i}}{\delta_2 x_i} \right) \sim -\frac{\Delta t}{4} \frac{\partial^4 \phi}{\partial x_i^4} \Delta x_i^2 = O(\Delta t^2 \Delta x_i^2), \quad (4.24)$$

where $\phi = O(\Delta t)$ is used. The error of the continuity equation $\delta_2 u_i^{n+1,m+1} / \delta_2 x_i = 0$ is the second-order accuracy in time and space.

When using Eq. (4.22), oscillation may occur in pressure distribution. To avoid spurious errors of pressure, using Rhie–Chow pressure interpolation (Rhie and Chow, 1983), the velocity $\hat{U}_i^{n+1,m+1}$ at the cell interface is given as

$$\hat{U}_i^{n+1,m+1} = \overline{\hat{u}_i^{n+1,m+1}}^{x_i} + \Delta t \lambda \frac{\overline{\delta_2 p^{n+1,m}}^{x_i}}{\delta_2 x_i} - \Delta t \lambda \frac{\delta_1 p^{n+1,m}}{\delta_1 x_i}. \quad (4.25)$$

When the pressure at the cell center (i, j, k) is expanded into a Taylor series, Eq. (4.25) can be rewritten as follows:

$$\hat{U}_i^{n+1,m+1} = \overline{\hat{u}_i^{n+1,m+1}}^{x_i} + \Delta t \frac{\Delta x_i^2}{4} \frac{\partial^3 p^{n+1,m}}{\partial x_i^3} + O(\Delta x_i^4). \quad (4.26)$$

The cell interface velocities contain errors of the first order in time and second order in space.

Using Eqs. (4.17), (4.20), and (4.25), the continuity equation obtained by the cell center velocity is given as

$$\begin{aligned} \frac{\delta_2 u_i^{n+1,m+1}}{\delta_2 x_i} &= \frac{\delta_1 \overline{u_i^{n+1,m+1}}^{x_i}}{\delta_1 x_i} = \frac{\delta_1}{\delta_1 x_i} \left(\overline{\hat{u}_i^{n+1,m+1}}^{x_i} - \Delta t \lambda \frac{\overline{\delta_2 \phi^m}^{x_i}}{\delta_2 x_i} \right) \\ &= \frac{\delta_1}{\delta_1 x_i} \left(U_i^{n+1,m+1} - \Delta t \lambda \frac{\overline{\delta_2 p^{n+1,m}}^{x_i}}{\delta_2 x_i} + \Delta t \lambda \frac{\delta_1 p^{n+1,m}}{\delta_1 x_i} + \Delta t \lambda \frac{\delta_1 \phi^m}{\delta_1 x_i} - \Delta t \lambda \frac{\overline{\delta_2 \phi^m}^{x_i}}{\delta_2 x_i} \right) \\ &= \frac{\delta_1 U_i^{n+1,m+1}}{\delta_1 x_i} + \Delta t \lambda \frac{\delta_1}{\delta_1 x_i} \left(\frac{\delta_1 p^{n+1,m+1}}{\delta_1 x_i} - \frac{\overline{\delta_2 p^{n+1,m+1}}^{x_i}}{\delta_2 x_i} \right) \\ &\sim -\frac{\Delta t}{4} \frac{\partial^4 p}{\partial x_i^4} \Delta x_i^2 = O(\Delta t^1 \Delta x_i^2). \end{aligned} \quad (4.27)$$

The error of the continuity equation $\delta_2 u_i^{n+1,m+1} / \delta_2 x_i = 0$ is the first order accuracy for time and the second order for space.

We improve the interpolation of the velocity at a cell interface so that the errors concerning time are second-order accurate in the continuity equation $\delta_2 u_i^{n+1} / \delta_2$. The expression (4.16) is rewritten as

$$\frac{\hat{u}_i^{n+1,m+1} - u_i^n}{\Delta t} = H_i^{n+1,m+1} - \lambda \frac{\delta_2(p^{n+1,m} - p^n)}{\delta_2 x_i} - \frac{\delta_2 p^n}{\delta_2 x_i}. \quad (4.28)$$

To find the velocity at the cell interface, we use the second term on the right-hand side of the above equation. The velocity $\hat{U}_i^{n+1,m+1}$ at the cell interface is obtained using the pressure difference $\Delta p^{n+1,m} = p^{n+1,m} - p^n$ as follows:

$$\hat{U}_i^{n+1,m+1} = \overline{\hat{u}_i^{n+1,m+1}}^{x_i} + \Delta t \lambda \frac{\overline{\delta_2 \Delta p^{n+1,m}}^{x_i}}{\delta_2 x_i} - \Delta t \lambda \frac{\delta_1 \Delta p^{n+1,m}}{\delta_1 x_i}. \quad (4.29)$$

This pressure difference weighted interpolation was also used in the study of Lee et al. (2019). Expanding the pressure difference Δp to a Taylor series, Eq. (4.29) is given as

$$\hat{U}_i^{n+1,m+1} = \overline{\hat{u}_i^{n+1,m+1}}^{x_i} + \Delta t \frac{\Delta x_i^2}{4} \frac{\partial^3 \Delta p^{n+1,m}}{\partial x_i^3} + O(\Delta x_i^4). \quad (4.30)$$

Because of $\Delta p^{n+1,m} = p^{n+1,m} - p^n = O(\Delta t)$, the error in the cell interface velocity is the second-order accuracy for both time and space. The method using Rhie–Chow pressure interpolation (Rhie and Chow, 1983) shown in Eq. (4.25) contains errors of first-order accuracy in time. However, using the Eq. (4.29), the time discretization is second-order accuracy. In this research, Newton iteration is not performed when obtaining steady fields. Therefore, we replace $\Delta p^{n+1,m}$ in Eq. (4.29) with $p^{n+1,m}$. In other words, Eq. (4.25) is used to interpolate the cell interface velocity.

Next, we evaluate the error of the continuity equation $\delta_2 u_i / \delta_2 x_i = 0$ determined by the velocity at the cell center. Using Eqs. (4.17), (4.20), and (4.29), the continuity formula is given as

$$\begin{aligned} \frac{\delta_2 u_i^{n+1,m+1}}{\delta_2 x_i} &= \frac{\overline{\delta_1 u_i^{n+1,m+1}}^{x_i}}{\delta_1 x_i} = \frac{\delta_1}{\delta_1 x_i} \left(\overline{\hat{u}_i^{n+1,m+1}}^{x_i} - \Delta t \lambda \frac{\overline{\delta_2 \phi^m}^{x_i}}{\delta_2 x_i} \right) \\ &= \frac{\delta_1}{\delta_1 x_i} \left(U_i^{n+1,m+1} - \Delta t \lambda \frac{\overline{\delta_2 \Delta p^{n+1,m}}^{x_i}}{\delta_2 x_i} + \Delta t \lambda \frac{\delta_1 \Delta p^{n+1,m}}{\delta_1 x_i} + \Delta t \lambda \frac{\delta_1 \phi^m}{\delta_1 x_i} - \Delta t \lambda \frac{\overline{\delta_2 \phi^m}^{x_i}}{\delta_2 x_i} \right) \\ &= \frac{\delta_1 U_i^{n+1,m+1}}{\delta_1 x_i} + \Delta t \lambda \frac{\delta_1}{\delta_1 x_i} \left(\frac{\delta_1 (p^{n+1,m+1} - p^n)}{\delta_1 x_i} - \frac{\overline{\delta_2 (p^{n+1,m+1} - p^n)}^{x_i}}{\delta_2 x_i} \right) \\ &\sim -\frac{\Delta t}{4} \frac{\partial^4 \Delta p}{\partial x_i^4} \Delta x_i^2 = O(\Delta t^2 \Delta x_i^2), \end{aligned} \quad (4.31)$$

where $\Delta p^{n+1} = p^{n+1} - p^n = O(\Delta t)$ after the Newton iteration finishes. The error of the continuity formula $\delta_2 u_i^{n+1} / \delta_2 x_i = 0$ is the second-order accuracy in both time and space.

In the collocation method, the velocity and pressure are obtained so as to satisfy the continuity equation (4.10) obtained from the velocity at the cell interface. Therefore, the continuity equation (4.9) obtained from the velocity at the cell center is not satisfied. Here, we consider a method that satisfies the two continuity equations. The pressure p is calculated from the Poisson equation (4.19) so as to satisfy the continuity equation (4.9). Furthermore, the pressure p_f is obtained from the Poisson equation (4.21) so as to satisfy the continuity equation (4.10). Similar to Rhie–Chow pressure interpolation (Rhie and Chow, 1983), we define the velocity $\hat{U}_i^{n+1,m+1}$ at the cell interface as follows:

$$\hat{U}_i^{n+1,m+1} = \overline{\hat{u}_i^{n+1,m+1}}^{x_i} + \Delta t \lambda \frac{\overline{\delta_2 p^{n+1,m}}^{x_i}}{\delta_2 x_i} - \Delta t \lambda \frac{\delta_1 p_f^{n+1,m}}{\delta_1 x_i}. \quad (4.32)$$

Two pressures are used in the above equation to interpolate the velocity at the cell interface. Expanding the pressure at the cell center (i, j, k) into a Taylor series, Eq. (4.32) can be rewritten as

$$\hat{U}_i^{n+1,m+1} = \overline{\hat{u}_i^{n+1,m+1}}^{x_i} + \Delta t \left(\frac{7 \Delta x_i^2}{24} \frac{\partial^3 p^{n+1,m}}{\partial x_i^3} + \frac{\partial p^{n+1,m}}{\partial x_i} \right) - \Delta t \left(\frac{\Delta x_i^2}{24} \frac{\partial^3 p_f^{n+1,m}}{\partial x_i^3} + \frac{\partial p_f^{n+1,m}}{\partial x_i} \right) + O(\Delta x_i^4). \quad (4.33)$$

The error includes $\partial p^{n+1,m}/\partial x_i$ and $\partial p_f^{n+1,m}/\partial x_i$. If $p = p_f$, the error terms of these first derivatives cancel each other out. Then, the velocity at the cell interface contains the errors of the first order in time and the second order in space.

Using Eqs. (4.17), (4.20), and (4.32), the continuity equation obtained by the cell center velocity is given as

$$\begin{aligned}
 \frac{\delta_2 u_i^{n+1,m+1}}{\delta_2 x_i} &= \frac{\delta_1 \overline{u_i^{n+1,m+1}}^{x_i}}{\delta_1 x_i} = \frac{\delta_1}{\delta_1 x_i} \left(\overline{u_i^{n+1,m+1}}^{x_i} - \Delta t \lambda \frac{\overline{\delta_2 \phi^m}^{x_i}}{\delta_2 x_i} \right) \\
 &= \frac{\delta_1}{\delta_1 x_i} \left(U_i^{n+1,m+1} - \Delta t \lambda \frac{\overline{\delta_2 p^{n+1,m}}^{x_i}}{\delta_2 x_i} + \Delta t \lambda \frac{\delta_1 p_f^{n+1,m}}{\delta_1 x_i} + \Delta t \lambda \frac{\delta_1 \phi^m}{\delta_1 x_i} - \Delta t \lambda \frac{\overline{\delta_2 \phi^m}^{x_i}}{\delta_2 x_i} \right) \\
 &= \frac{\delta_1 U_i^{n+1,m+1}}{\delta_1 x_i} + \Delta t \lambda \frac{\delta_1}{\delta_1 x_i} \left(\frac{\delta_1 p_f^{n+1,m+1}}{\delta_1 x_i} - \frac{\overline{\delta_2 p^{n+1,m+1}}^{x_i}}{\delta_2 x_i} \right) \\
 &\sim \Delta t \left(\frac{1}{12} \frac{\partial^4 p_f}{\partial x_i^4} \Delta x_i^2 + \frac{\partial^2 p_f}{\partial x_i^2} \right) - \Delta t \left(\frac{1}{3} \frac{\partial^4 p}{\partial x_i^4} \Delta x_i^2 + \frac{\partial^2 p}{\partial x_i^2} \right). \tag{4.34}
 \end{aligned}$$

For $p = p_f$, the continuity formula (4.34) agrees with Eq. (4.27). Then the continuity formula is $\delta_2 u_i^{n+1,m+1}/\delta_2 x_i = O(\Delta t^1 \Delta x_i^2)$, and the error is the first-order accuracy for time and the second-order accuracy for space.

We refine the interpolation of the cell interface velocity so that the error in the continuity equation $\delta_2 u_i^{n+1,m+1}/\delta_2 x_i = 0$ to time is second-order accurate. We replace the pressures p and p_f with the pressure differences Δp and Δp_f in Eq. (4.32). The velocity $\hat{U}_i^{n+1,m+1}$ at the cell interface is given as

$$\hat{U}_i^{n+1,m+1} = \overline{u_i^{n+1,m+1}}^{x_i} + \Delta t \lambda \frac{\overline{\delta_2 \Delta p^{n+1,m}}^{x_i}}{\delta_2 x_i} - \Delta t \lambda \frac{\delta_1 \Delta p_f^{n+1,m}}{\delta_1 x_i}. \tag{4.35}$$

It is found that using the Taylor series expansion, the velocity at the cell interface contains the errors of the second order in time. In addition, the error in the continuity formula $\delta_2 u_i^{n+1,m+1}/\delta_2 x_i = 0$ given by the velocity at the cell center is the second-order accuracy in time.

We should calculate two Poisson equations to obtain two pressures for the pressure interpolation using Eq. (4.32). Therefore, it leads to an increase in computation time. As a result of numerical experiments, when $p \approx p_f$, two continuity equations (4.9) and (4.10) could be satisfied at the same time. However, if we changed the Courant number, $p \approx p_f$ did not hold, and no convergent solution was obtained. At present, we have not established a method that simultaneously satisfies the two continuity equations. Further investigation is necessary in the future.

5 Numerical method

An overview of the method of solving Eqs. (2.1) and (2.2) in the Cartesian coordinate system was given in Section 4. Equations (3.3) and (3.4) transformed to general curvilinear coordinates are solved similarly. Herein, we describe a method for the simultaneous relaxation of velocity and pressure. The technique is the same as the simultaneous relaxation method used by the authors (Yanaoka and Inafune, 2023; Yanaoka, 2023), and the existing process is extended to the general curvilinear coordinate system. The Newton method is used to solve the unsteady solution. Applying the implicit midpoint rule to Eqs. (3.3) and (3.4), the respective equations are given as

$$\frac{u_i^{n+1,m+1} - u_i^n}{\Delta t} = H_i^{n+\lambda,m+1} - \frac{\partial \xi_m}{\partial x_i} \frac{\partial p^{n+\lambda,m+1}}{\partial \xi_m}, \tag{5.1}$$

$$\frac{T^{n+1,m+1} - T^n}{\Delta t} = H_T^{n+\lambda,m+1}, \tag{5.2}$$

$$H_i^{n+\lambda,m+1} = -\frac{1}{J} \frac{\partial}{\partial \xi_m} (J U_m^{n+\lambda,m+1} u_i^{n+\lambda,m+1}) + \frac{1}{Re} \frac{1}{J} \frac{\partial}{\partial \xi_m} \left(J g_{mn} \frac{\partial u_i^{n+\lambda,m+1}}{\partial \xi_n} \right) - \frac{Ra}{Re^2 Pr} T^{n+\lambda,m+1} e_i, \tag{5.3}$$

$$H_T^{n+\lambda,m+1} = -\frac{1}{J} \frac{\partial}{\partial \xi_m} (J U_m^{n+\lambda,m+1} T^{n+\lambda,m+1}) + \frac{1}{Re Pr} \frac{\partial}{\partial \xi_m} \left(J g_{mn} \frac{\partial T^{n+\lambda,m+1}}{\partial \xi_n} \right), \tag{5.4}$$

$$u_i^{n+\lambda,m+1} = \lambda u_i^{n+1,m+1} + (1-\lambda) u_i^n, \tag{5.5}$$

$$JU_m^{n+\lambda, m+1} = \lambda JU_m^{n+1, m+1} + (1 - \lambda) JU_m^n, \quad (5.6)$$

$$p^{n+\lambda, m+1} = \lambda p^{n+1, m+1} + (1 - \lambda) p^n, \quad (5.7)$$

$$T^{n+\lambda, m+1} = \lambda T^{n+1, m+1} + (1 - \lambda) T^n, \quad (5.8)$$

where the superscripts n and m indicate the time and Newton iterative levels, respectively. This study uses the Euler implicit method ($\lambda = 1$) for steady field analysis and the implicit midpoint rule ($\lambda = 1/2$) for unsteady field analysis. Spatial derivatives are discretized with second-order accuracy central differences using the method described in Section 4.

We use a collocated grid in a general curvilinear coordinate system. Applying the SMAC method (Amsden and Harlow, 1970), Eq. (5.1) is temporally split as follows:

$$\frac{\hat{u}_i^{n+1, m+1} - u_i^n}{\Delta t} = H_i^{n+\lambda, m+1} - \frac{\partial \xi_m}{\partial x_i} \frac{\partial}{\partial \xi_m} [\lambda p^{n+1, m} + (1 - \lambda) p^n], \quad (5.9)$$

$$\frac{u_i^{n+1, m+1} - \hat{u}_i^{n+1, m+1}}{\Delta t} = -\lambda \frac{\partial \xi_m}{\partial x_i} \frac{\partial \phi^m}{\partial \xi_m}, \quad (5.10)$$

$$p^{n+1, m+1} = p^{n+1, m} + \phi^m, \quad (5.11)$$

where $\hat{u}_i^{n+1, m+1}$ is the predicted value of velocity, and ϕ^m is the pressure correction value.

Next, we must obtain the contravariant velocity JU_m^{n+1} at the cell interface to derive the Poisson equation for the pressure correction value. From the contravariant velocity definition equation (3.6) and the velocity correction equation (5.10), the following equation is obtained:

$$JU_m^{n+1, m+1} = \hat{JU}_m^{n+1, m+1} - \Delta t \lambda \left(Jg_{mn} \frac{\partial \phi^m}{\partial \xi_n} \right). \quad (5.12)$$

As the predicted velocity value \hat{u}_i is defined at the cell center, we must find \hat{u}_i at the cell interface by interpolation to obtain \hat{JU}_m . Using the pressure interpolation by Rhie–Chow (Rhie and Chow, 1983), the velocity at the cell interface can be defined as

$$\hat{JU}_m^{n+1, m+1} = \langle JU_m^{n+1, m+1} \rangle - \Delta t \lambda Jg_{mm} \left(\frac{\partial p^{n+1, m}}{\partial \xi_m} - \left\langle \frac{\partial p^{n+1, m}}{\partial \xi_m} \right\rangle \right), \quad (5.13)$$

where $\langle \rangle$ represents the interpolated value at the cell interface.

In this study, as explained in Section 4, we Interpolate the velocity at the cell interface using the pressure difference $\Delta p^{n+1, m} = p^{n+1, m} - p^n$ as follows:

$$\hat{JU}_m^{n+1, m+1} = \langle JU_m^{n+1, m+1} \rangle - \Delta t \lambda Jg_{mm} \left(\frac{\partial \Delta p^{n+1, m}}{\partial \xi_m} - \left\langle \frac{\partial \Delta p^{n+1, m}}{\partial \xi_m} \right\rangle \right). \quad (5.14)$$

Taking the divergence of Eq. (5.12) and using the continuity equation (3.2) at the $n + 1$ level, the following Poisson equation for the pressure correction value ϕ is derived as

$$\lambda \frac{\partial}{\partial \xi_m} \left(Jg_{mn} \frac{\partial \phi^m}{\partial \xi_n} \right) = \frac{1}{\Delta t} \frac{\partial \hat{JU}_m^{n+1, m+1}}{\partial \xi_m}. \quad (5.15)$$

Equations (5.9), (5.10), (5.11), (5.14), and (5.15) are used when the collocation method is applied to the SMAC method (Amsden and Harlow, 1970) in a general curvilinear coordinate system. When the Poisson equation in the above formula (5.15) is discretized, coefficients of nine components appear in a two-dimensional case and 19 components in a three-dimensional case. Therefore, it takes much time to iterate the Poisson equation. In this study, to reduce memory usage and simplify the calculation of the Poisson equation, we omit the differential term in which the cross term Jg_{mn} appears. Simply omitting the cross term will require under-relaxation when solving the Poisson equation using an iterative method such as the successive over-relaxation (SOR) method. Therefore, in this study, we adopt the idea of the highly simplified marker and cell (HSMAC) method (Hirt et al., 1975) and perform simultaneous relaxation of velocity and pressure to prevent under-relaxation. We simplify the Poisson equation for pressure correction value as follows:

$$\lambda \frac{\partial}{\partial \xi_m} \left(Jg_{mm} \frac{\partial \phi^{m, l}}{\partial \xi_m} \right) = \frac{1}{\Delta t} \frac{\partial JU_m^{n+1, m+1, l}}{\partial \xi_m}. \quad (5.16)$$

Velocity and pressure are modified as follows: Note that the cross term in the velocity correction equation is not omitted:

$$JU_m^{n+1,m+1,l+1} = JU_m^{n+1,m+1,l} - \Delta t \lambda \left(Jg_{mn} \frac{\partial \phi^{m,l}}{\partial \xi_n} \right), \quad (5.17)$$

$$u_i^{n+1,m+1,l+1} = u_i^{n+1,m+1,l} - \Delta t \lambda \left(\frac{\partial \xi_m}{\partial x_i} \frac{\partial \phi^{m,l}}{\partial \xi_m} \right), \quad (5.18)$$

$$p^{n+1,m+1,l+1} = p^{n+1,m+1,l} + \phi^{m,l}, \quad (5.19)$$

where the superscript l is the number of iterations. When $l = 1$, let $JU_m^{n+1,m+1,l} = \hat{J}U_m^{n+1,m+1}$, $u_i^{n+1,m+1,l} = \hat{u}_i^{n+1,m+1}$, and $p^{n+1,m+1,l} = p^{n+1,m+1}$, the velocity and pressure are simultaneously relaxed. We repeat the calculation up to a predetermined iteration number. After the simultaneous relaxation is completed, we let $JU_m^{n+1,m+1} = JU_m^{n+1,m+1,l+1}$, $u_i^{n+1,m+1} = u_i^{n+1,m+1,l+1}$, and $p^{n+1,m+1} = p^{n+1,m+1,l+1}$. Takemitsu (Takemitsu, 1985) proposed a similar method that simultaneously iterates the velocity correction equation and the Poisson equation of the pressure correction. However, the Poisson equation for pressure should be solved after correcting the velocity. The present numerical method does not require solving the Poisson equation for the pressure. It is significant to include the cross term in the velocity correction equation (5.18). By simultaneously relaxing velocity and pressure, the influence of the cross term is considered for the velocity and pressure, and the velocity is corrected to satisfy the continuity equation. With such simultaneous relaxation, the Poisson equation can be solved without under-relaxation. However, the use of the SOR method is inconvenient because the optimal value of the acceleration relaxation coefficient changes depending on the number of grid points and the flow field. In this study, we used the biconjugate gradient stabilized method (Van der Vorst, 1992) to solve simultaneous linear equations.

A boundary condition is required when solving the Poisson equation (5.16) for pressure correction value. In this study, as the velocity and pressure are simultaneously relaxed while solving the Poisson equation, the boundary condition of the pressure correction value is simplified. If $JU_m^{n+1,l+1} = JU_m^{n+1,l}$ at the boundary, then $Jg_{mn} \partial \phi^{m,l} / \partial \xi_n = 0$ is obtained. Considering that the pressure correction value ϕ asymptotically approaches zero with iteration, and omitting the influence of the cross term, the condition for first derivative zero, $\partial \phi^{m,l} / \partial \xi_n = 0$, at the boundary is obtained. Because ϕ asymptotically approaches zero with iteration, the effect of this approximation on the inside of the computational domain is considered to be small.

These discretized equations are solved following the next procedure.

- Step 1: At $m = 1$, let $u_i^{n+1,m} = u_i^n$, $p^{n+1,m} = p^n$, and $T^{n+1,m} = T^n$.
- Step 2: Solve Eq. (5.9), and predict the velocity $\hat{u}_i^{n+1,m+1}$.
- Step 3: Interpolate the cell interface velocity $\hat{J}U_m^{n+1,m+1}$ from Eq. (5.14).
- Step 4: The Poisson equation (5.16) for pressure correction value ϕ^m , and velocity and pressure correction equations (5.17), (5.18), (5.19) are simultaneously relaxed. At the end of simultaneous relaxation, set $JU_m^{n+1,m+1}$, $u_i^{n+1,m+1}$, and $p^{n+1,m+1}$.
- Step 5: Solve Eq. (5.2) and find the temperature $T^{n+1,m+1}$.
- Step 6: Repeat Steps 2 to 5. After the Newton iteration is completed, set $u_i^{n+1} = u_i^{n+1,m+1}$, $p^{n+1} = p^{n+1,m+1}$, and $T^{n+1} = T^{n+1,m+1}$.
- Step 7: Advance the time step and return to Step 1.

6 Verification of numerical method

This research first analyzes steady fields and verifies the validity of this numerical method. In addition, we confirm that pressure oscillation does not occur. Next, we analyze unsteady fields and investigate the influence of weighted interpolation by pressure difference on the calculation accuracy.

6.1 Natural convection inside a cavity

We analyze natural convection in a square cavity and compare our results with existing results. The origin is placed at the bottom of the container, the x - and y -axes are in the horizontal and vertical directions, respectively, and the z -axis is perpendicular to the plane of the paper. The length of one side of the container is H , and all boundaries are surrounded by walls. A non-slip boundary condition is applied to the wall surface. The left and right wall surfaces are heated and cooled at uniform temperatures T_H and T_C , respectively. Adiabatic conditions are imposed on the upper and lower wall surfaces. The pressure is obtained by second-order accuracy extrapolation. Periodic boundaries

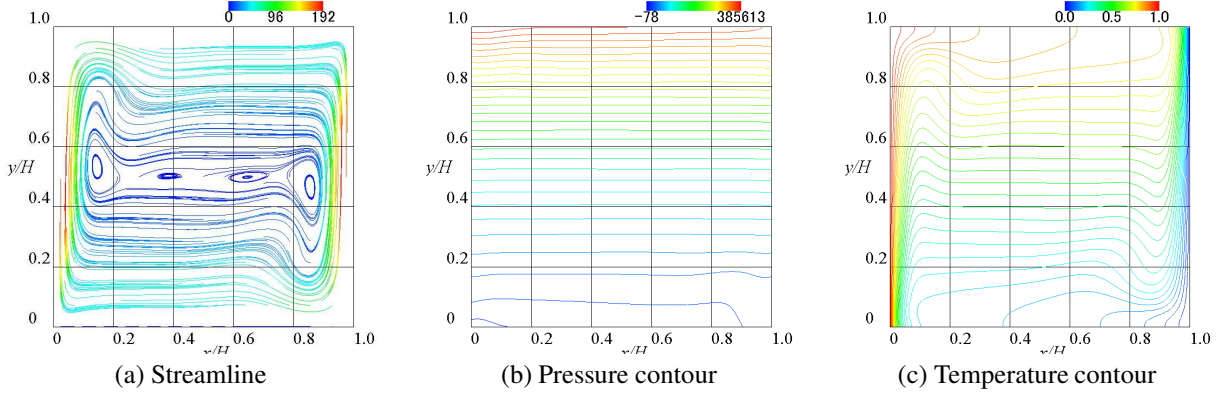
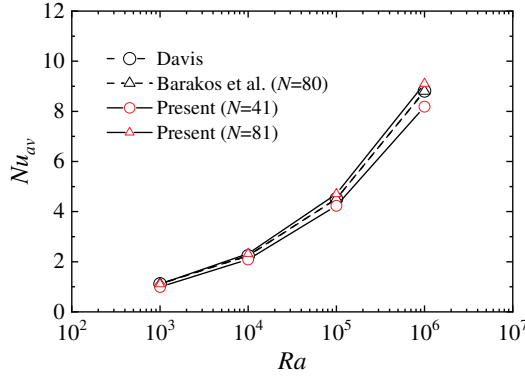

 Figure 1: Flow field at $Ra = 1 \times 10^6$ for a square cavity model


Figure 2: Average Nusselt number for a square cavity model

are imposed in the z -direction for the velocity, pressure, and temperature. The grid used is a $N \times N \times 2$ non-uniform grid, which is generated using the following function:

$$x_i = \frac{1}{2} \frac{\tanh(\alpha\eta)}{\tanh(\alpha)}, \quad \eta = 2 \frac{i-1}{N-1} - 1, \quad (6.1)$$

where i represents a grid point and $\alpha = 1$. The y -coordinate is also generated using the same function. Grid points with $N = 41$ and 81 are used for this analysis. The minimum grid widths in each grid are $\Delta_{\min} = 0.001H$ and $0.0005H$, respectively. The computational region in the z -direction is set to the minimum grid width. The reference values used for non-dimensionalization are $l_{\text{ref}} = H$, $u_{\text{ref}} = \alpha/H$, and $T_{\text{ref}} = T_C$. The temperature difference is defined as $\Delta T = T_H - T_C$. In this calculation, to compare with existing studies (De Vahl Davis, 1983; Barakos et al., 1994), the Rayleigh numbers are set to $Ra = 10^3, 10^4, 10^5$, and 10^6 . The Prandtl number is $Pr = 0.71$. The Courant number is $CFL = \Delta t u_{\text{ref}} / \Delta_{\min} = 0.2$.

Figure 1 shows the streamlines, pressure, and temperature distributions at $Ra = 10^6$. Fluid heated near the hot wall is pushed up by buoyancy and transported to the cold wall. On the other hand, the transported high-temperature fluid descends while being cooled by the low-temperature wall and flows into the high-temperature wall side again. A clockwise heat convection is generated by a series of such movements of the fluid. The flow and temperature fields obtained using this computational method are qualitatively similar to the existing result (De Vahl Davis, 1983; Barakos et al., 1994). No oscillations are seen in the pressure distribution.

In Fig. 2, the average Nusselt number Nu_{av} on the heating surface is compared with the existing values (De Vahl Davis, 1983; Barakos et al., 1994). In the case of $N = 41$, this calculated value is lower than the previous ones and is underestimated compared with the earlier studies. For $N = 81$, the present result agrees well with the existing ones. It was found from the above results that this computational method can predict the heat transfer characteristics at high Rayleigh numbers.

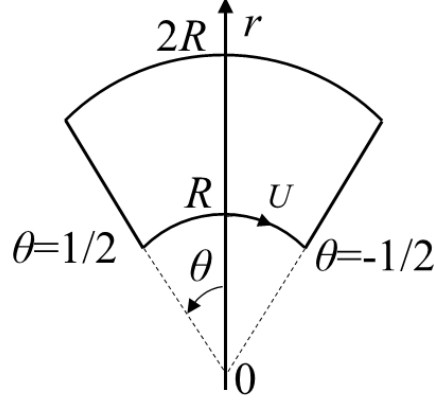


Figure 3: Geometry of a polar cavity model

6.2 Flow in a polar cavity

Analysis of the flow inside the polar cavity has been carried out in existing studies (Zang et al., 1994; Wu et al., 1995; Fuchs and Tillmark, 1985; Rosenfeld et al., 1991) to verify the numerical method. Figure 3 shows the geometry of the polar cavity model. The r - and θ -axes are in the radial and circumferential directions, respectively, and the z -axis is perpendicular to the plane of the paper. All boundaries are enclosed by walls. The internal fluid is driven by the wall moving with uniform velocity U at radius $r = R$. Non-slip boundary conditions are given for other wall surfaces. The pressure is obtained by second-order accuracy extrapolation. Periodic boundary conditions are imposed in the z -direction for velocity and pressure. The grid used is a $N \times N \times 2$ non-uniform grid, which is generated using the following function:

$$r_j = R + \frac{1}{2} \frac{\tanh(\alpha \eta_r)}{\tanh(\alpha)}, \quad \eta_r = 2 \frac{j-1}{N-1} - 1, \quad (6.2)$$

$$\theta_i = \frac{1}{2} \frac{\tanh(\alpha \eta_\theta)}{\tanh(\alpha)}, \quad \eta_\theta = 2 \frac{i-1}{N-1} - 1, \quad (6.3)$$

$$x_{i,j} = r_j \sin(\theta_i), \quad y_{i,j} = r_j \cos(\theta_i), \quad (6.4)$$

where i and j represent grid points and $\alpha = 1$. Grid points with $N = 41$ and 81 are used for this analysis. The minimum grid widths in the radial and circumferential directions are $\Delta_{\min} = 0.01R$ and $0.005R$ for $N = 41$ and 81 , respectively. The computational domain in the z -direction is $0.01R$. The reference values used for non-dimensionalization are $l_{\text{ref}} = R$ and $u_{\text{ref}} = U$. In this calculation, the Reynolds number is set to $Re = 350$ to compare with existing research (Wu et al., 1995; Fuchs and Tillmark, 1985). The Courant number is $CFL = \Delta t U / \Delta_{\min} = 1$.

Streamlines and pressure contours are shown in Fig. 4. There is a large-scale vortex at the center of the flow field and secondary vortices at the corners. These computational results agree well with the flow visualization experiments of Fuchs and Tillmark (1985). In addition, no vibration occurs in the pressure distribution. In this model, pressure oscillation did not appear even without using the Rhie–Chow interpolation.

Figure 5 shows the radial velocity u_r and circumferential velocity u_θ at $\theta = -20^\circ, 0^\circ, 20^\circ$. The experimental and calculated values of Fuchs and Tillmark (1985) are compared. The results obtained using the grid with $N = 41$ and $N = 81$ agree, and there is no grid dependency on the calculation results. This calculation result is in good agreement with the previous experimental value. The existing calculation results were obtained using a grid of 80×80 . Although the present calculation results were obtained using about half the grid points compared to the previous calculation, the distributions for all θ agree well with the existing values.

6.3 Flow in a skewed cavity

Next, to verify the accuracy of this numerical method in non-orthogonal grids, we analyze the flow in a skewed cavity, similar to existing research (Perić, 1990; Wu et al., 1995). Figure 6 shows the geometry of the skewed cavity model. The x - and y -axes are in the horizontal and vertical directions, respectively, and the z -axis is perpendicular to the plane of the paper. The walls on both sides are inclined at an angle β , and the cavity has a width of a and a height of $h = a \tan \beta$. As for the boundary conditions, the upper wall moves with a uniform velocity U , and non-slip boundary conditions are given for other wall surfaces. The pressure is obtained by second-order accuracy extrapolation. Periodic

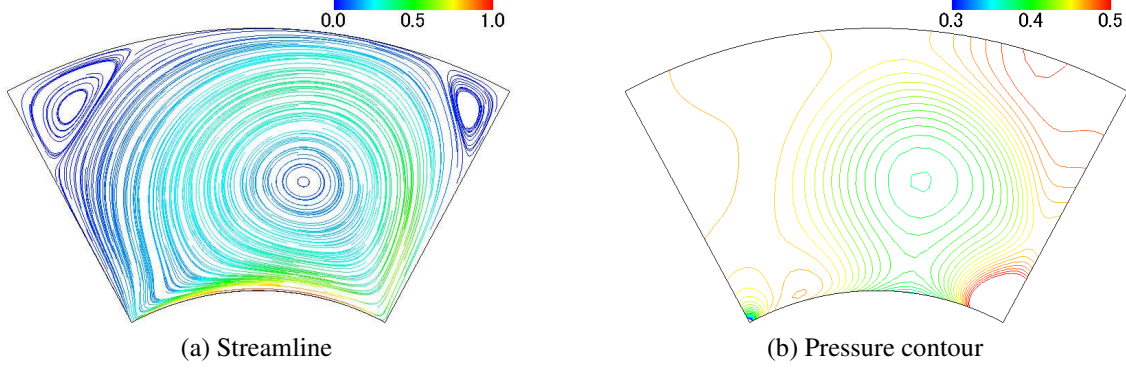
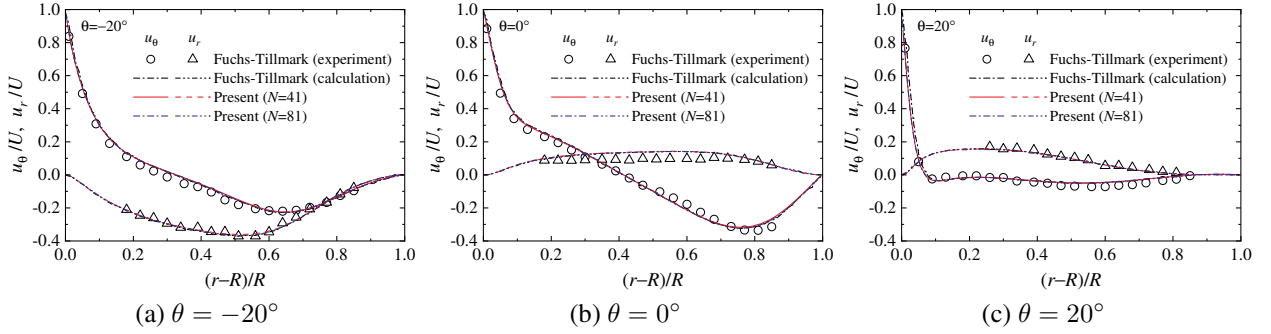
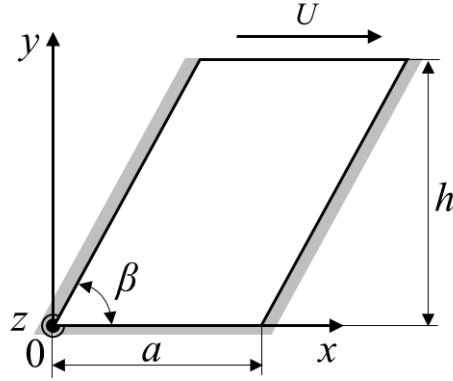

 Figure 4: Flow field at $Re = 350$ for a polar cavity model

 Figure 5: Velocity profiles along radial lines at $Re = 350$ for a polar cavity model


Figure 6: Geometry of a skewed cavity model

boundary conditions are imposed in the z -direction for velocity and pressure. In this calculation, we analyze the case of $\beta = 30^\circ$ and 45° . The grid used for the calculation is a non-uniform grid of $61 \times 61 \times 2$ and was generated using the same functions as the formulas (6.2) and (6.3). The minimum grid width is $\Delta y_{\min} = 0.0054a$ and $0.0094a$ for $\beta = 30^\circ$ and 45° , respectively. The computational area in the z -direction is $0.01a$. The number of grid points in the x - y cross-section is the same as that used in the calculation of Wu et al. (1995). The reference values used for non-dimensionalization are $l_{\text{ref}} = a$ and $u_{\text{ref}} = U$. In this calculation, the Reynolds number is set to $Re = 100$ to compare with existing research (Perić, 1990; Wu et al., 1995). The time step is $\Delta t/(a/U) = 0.005$, and the Courant number defined as $CFL = \Delta t U / \Delta_{\min}$ is $CFL = 0.92$ and 0.53 for $\beta = 30^\circ$ and 45° , respectively.

The streamlines and pressure contours at $\beta = 45^\circ$ are shown in Fig. 7. Large-scale and secondary vortices exist at the upper and lower of the flow field, respectively. This result qualitatively agrees well with the calculation result of Perić (1990); Wu et al. (1995). In addition, no oscillations occur in the pressure distribution. In this model, pressure oscillations appeared without the Rhie–Chow interpolation.

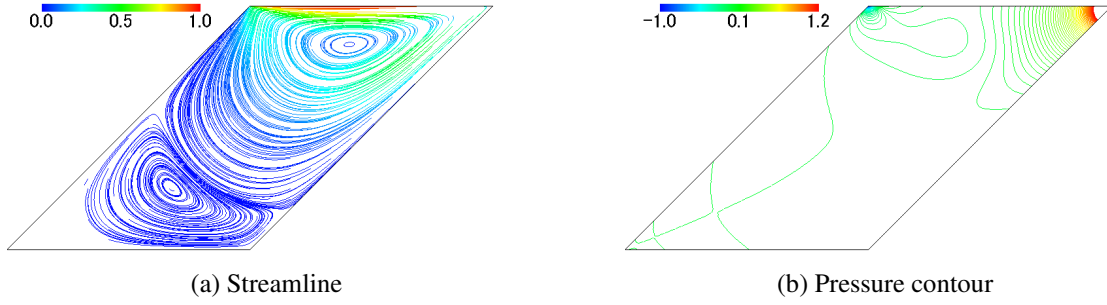
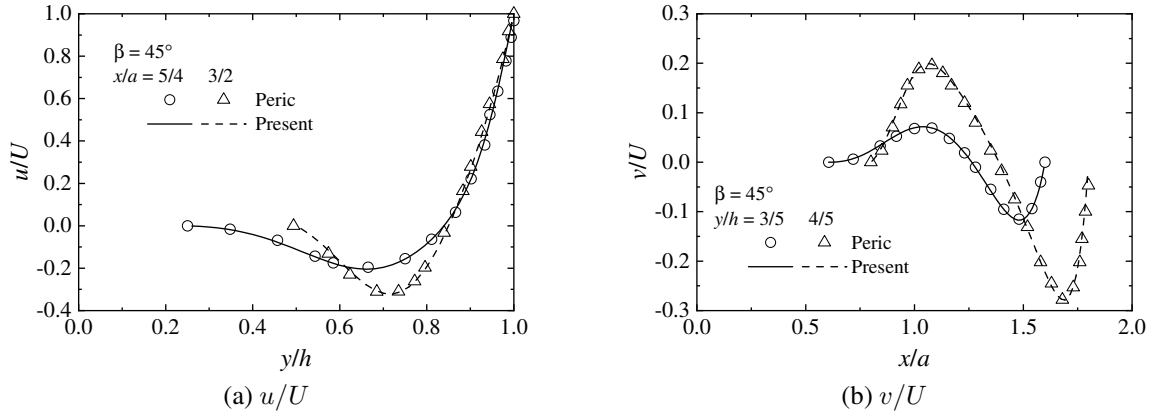
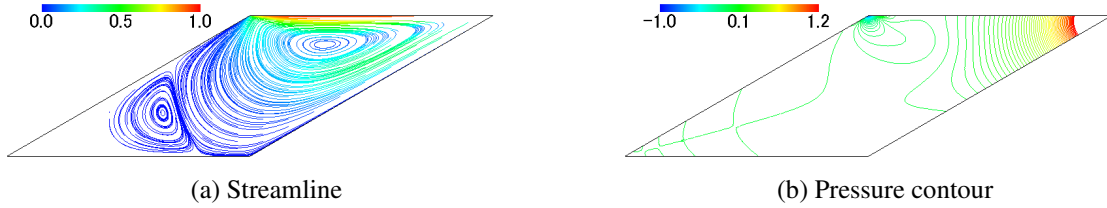

 Figure 7: Flow field at $Re = 100$ and $\beta = 45^\circ$ for a skewed cavity model

 Figure 8: Horizontal and vertical velocity profiles at $Re = 100$ and $\beta = 45^\circ$ for a skewed cavity model

 Figure 9: Flow field at $Re = 100$ and $\beta = 30^\circ$ for a skewed cavity model

Figure 8 shows the horizontal velocities u at $x/a = 5/4$ and $3/2$, and the vertical velocities v at $y/h = 3/5$ and $4/5$. The calculated values of Perić (1990) are compared. The existing calculation results were obtained using a uniform cell of 80×80 . Although the present calculation results used fewer grid points than the existing calculations, they agree well with the existing results.

The streamlines and pressure contours at $\beta = 30^\circ$ are shown in Fig. 9. Similar to the result of $\beta = 45^\circ$, the flow field agrees well with the calculation result of Perić (1990). It can be seen that the vortices at the top of the cavity reach the bottom wall compared with the results for $\beta = 45^\circ$. In addition, no pressure oscillations occur.

Figure 10 shows the horizontal velocities u at $x/a = 5/4$ and $3/2$, and the vertical velocities v at $y/h = 1/3$ and $2/3$. The calculated values of Perić (1990) and Wu et al. (1995) are included for comparison. The study of Wu et al. (1995) showed the results when the cross-derivative term of the Poisson equation was included and ignored. Here, the results with the cross-derivative term are compared. The present result at $y/h = 2/3$ agrees well with that of Wu et al. (1995), although there is a slight difference from the result of Perić (1990). Overall, it can be said that the calculation results are valid. We also performed calculations without omitting the cross-derivative term and confirmed that the result matched the present calculated value.

Wu et al. (1995) reported that when calculating the Poisson equation without the cross term, there was a significant difference from the existing value (Perić, 1990). The simultaneous velocity and pressure relaxation method

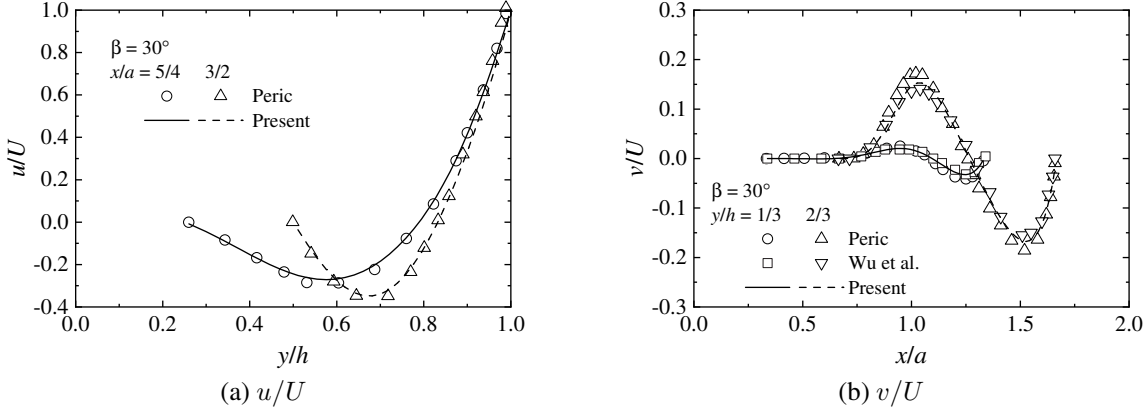


Figure 10: Horizontal and vertical velocity profiles at $Re = 100$ and $\beta = 30^\circ$ for a skewed cavity model

used in the present study provides good agreement with existing values even if the cross-derivative term is ignored. Furthermore, unlike the analysis of Perić (1990), it was found that we can perform the calculation stably without any under-relaxation. In addition, when calculating without omitting the cross-derivative term at $\beta = 30^\circ$, the execution time increased by approximately 31 compared to when the cross term was ignored. There is no difference in the decreasing tendency of the residuals of the continuity equations, and the residuals decrease to the same level with the same number of iterations. The present numerical method makes efficient calculations possible even if the cross-derivative term is omitted.

6.4 Taylor decaying vortex

For high Reynolds number flows with the decaying of kinetic energy, the accuracy of the present numerical method is verified by comparing the calculation result with the exact solution. A Taylor decaying vortex analysis is performed to verify the accuracy and convergence. The solution to the Taylor decaying vortex problem (Taylor, 1923) is given as

$$u = -\cos(kx) \sin(ky) e^{-\frac{2k^2}{Re}t}, \quad (6.5)$$

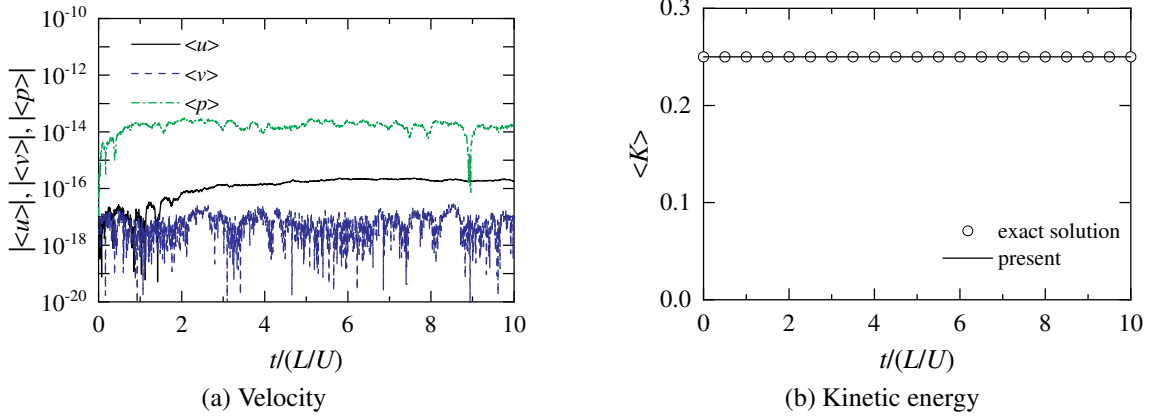
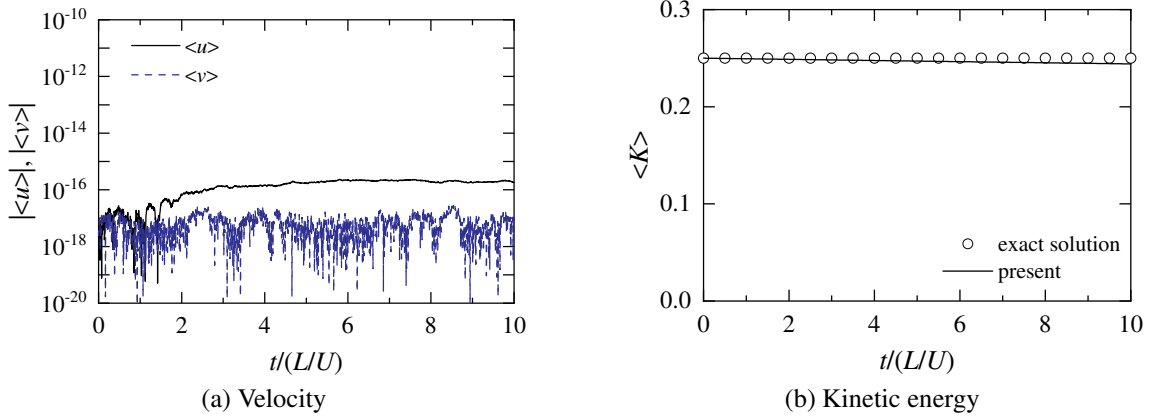
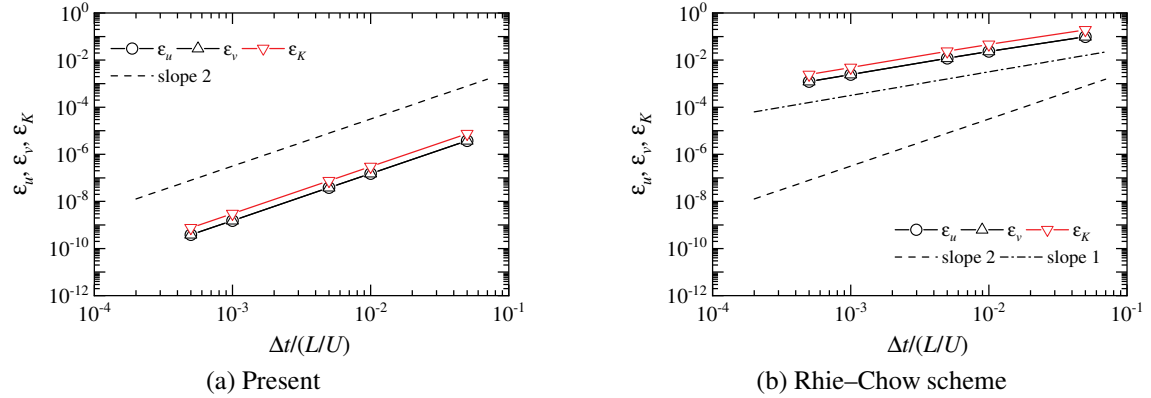
$$v = \sin(kx) \cos(ky) e^{-\frac{2k^2}{Re}t}, \quad (6.6)$$

$$p = -\frac{1}{4} [\cos(2kx) + \cos(2ky)] e^{-\frac{4k^2}{Re}t} \quad (6.7)$$

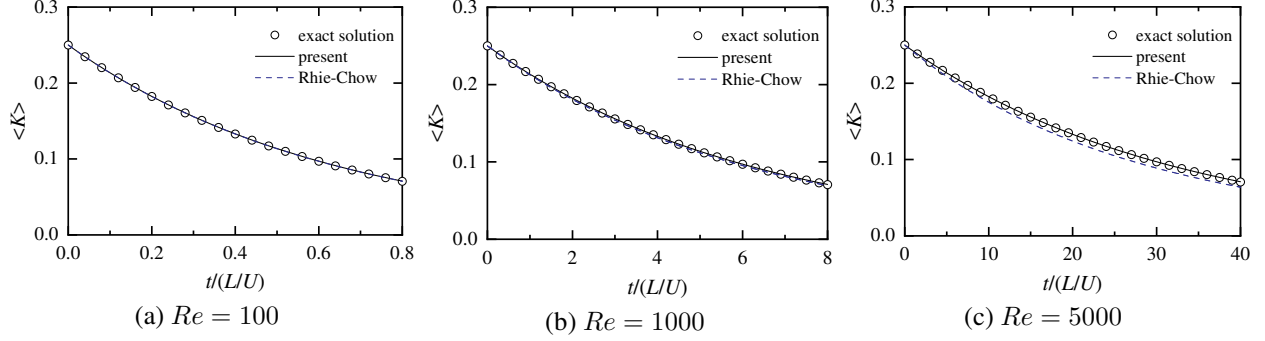
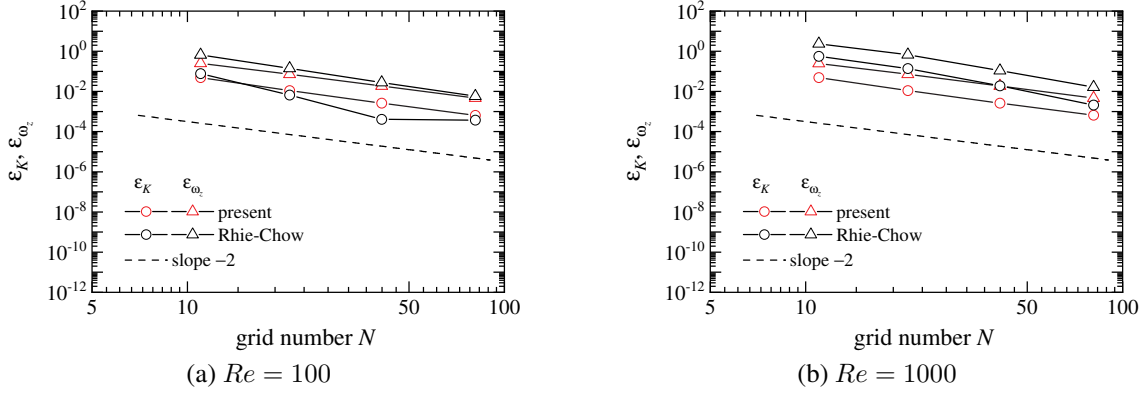
where $k = 2\pi$. These equations are non-dimensionalized by the maximum velocity U and the wavelength L of the periodic vortex.

The calculation area is $L \times L$, and the computational region in the z -direction is the grid spacing. The exact solution is given as the initial condition, and the periodic boundary is set as the boundary condition. A uniform grid with $N \times N \times 2$ is used. N is the number of grid points in the x - and y -directions. N is changed to $N = 11, 21, 41$, and 81 , and the convergence of the calculation results with respect to the number of grid points is investigated. The reference values used in this calculation are $l_{\text{ref}} = L$ and $u_{\text{ref}} = U$. The Reynolds number is changed to $Re = 10^2, 10^3$, and 5×10^3 . The Courant number is defined as $\text{CFL} = \Delta t U / \Delta x$ using the maximum velocity U and grid spacing Δx . For inviscid analysis, we use a grid of $N = 41$ and set the time step at which the Courant number becomes $\text{CFL} = 0.5$. In viscous analysis, the Courant number is $\text{CFL} = 0.4$ for each grid.

As this computational model is a periodic flow, the total amounts of momentum and kinetic energy are conserved for $Re = \infty$. Similar to existing research (Yanaoka, 2023), we investigate the conservation properties for momentum and kinetic energy. Figure 11(a) shows the total amount, $\langle u \rangle$ and $\langle v \rangle$, of velocity obtained using this numerical method. The total amount was determined by volume integration within the calculation domain. Each total amount is zero, as can be seen from the volume integral of the exact solution. All the total amounts remain at low levels, indicating excellent conservation of the velocity. The total amount, $\langle K \rangle$, of kinetic energy is shown in Fig. 11(b). This calculation result agrees well with the exact solution, and it can be seen that the energy is conserved. Figure 12 shows the results obtained by the Rhie–Chow scheme. Although the velocity is conserved, the total amount of kinetic energy deviates from its initial value over time. If $Re = \infty$, the initial value must be maintained. In the Rhie–Chow scheme, the kinetic energy contains a first-order accuracy error to time, which degrades the energy conservation property.


 Figure 11: Total amounts of velocity and kinetic energy at $Re = \infty$ using the present method for a decaying vortex

 Figure 12: Total amounts of velocity and kinetic energy at $Re = \infty$ using the Rhie-Chow scheme for a decaying vortex

 Figure 13: Errors of velocity and kinetic energy at $Re = \infty$ for a decaying vortex

The maximum velocity errors, ε_u and ε_v , and the relative error, ε_K , of kinetic energy are shown in Fig. 13. The relative error is defined as the relative difference from the initial value. When using this numerical method, the slope of the errors for velocity and kinetic energy is 2, and the error converges to second-order accuracy as the time step Δt decreases. On the other hand, the Rhie-Chow interpolation method does not show second-order convergence, and it is found that errors in first-order accuracy are included in velocity and kinetic energy.


 Figure 14: Kinetic energies at $Re = 100, 1000$, and 5000 for a decaying vortex: $N = 41$

 Figure 15: Variations of the relative error of kinetic energy and maximum error of vorticity with a number of grids using different interpolations at $Re = 1000$ for a decaying vortex

Next, we demonstrate the results of the viscous analysis. The total amount of kinetic energy at $Re = 100 - 5000$ is shown in Fig. 14. The number of grid points used is $N = 41$. For $Re = 100$ and 1000 , the results in both interpolation methods agree with the exact solution. In a flow dominated by viscosity, the influence of the first-order accuracy error contained in the kinetic energy does not appear in the time variation of the kinetic energy. At $Re = 5000$, there is a difference between the result by Rhie-Chow's method and the exact solution. At a high Reynolds number, the difference between the interpolation methods appears.

Figure 15 shows the relative error, $\epsilon_K = |(\langle K \rangle - \langle K \rangle_e) / \langle K \rangle_e|$, of the kinetic energy. Here, the subscript e represents the exact solution. The maximum error, ϵ_{ω_z} , of vorticity in the z -direction is also shown. When the Reynolds number is low, there is almost no difference between the interpolation methods. When the Reynolds number increases, the error of the present method is lower than that of the Rhie-Chow interpolation method. As the number of grid points increases, the error decreases with a slope of -2 , indicating second-order convergence.

As can be seen by substituting the exact solution into the Navier-Stokes equation (2.2), the time derivative term is canceled by the viscous term. Therefore, we could not confirm the effect of time increments on calculation accuracy in the viscosity analysis.

6.5 Periodic three-dimensional inviscid flow

In the Taylor decaying vortex model, when $Re = \infty$, the exact solution does not change over time, and the initial value is maintained. In this subsection, we analyze a three-dimensional inviscid flow in which the velocity and pressure change over time from the initial conditions.

As an initial condition for the three-dimensional flow field, the vector potential Ψ is given as

$$\Psi_x = \frac{1}{k} \sin(ky), \quad \Psi_y = \frac{1}{k} \sin(kz), \quad \Psi_z = \frac{1}{k} \sin(kx), \quad (6.8)$$

where $k = 2\pi$. Using the relationship $\mathbf{u} = \nabla \times \Psi$, the velocity can be obtained from Eq. (6.8) as follows:

$$u = -\cos(kz), \quad v = -\cos(kx), \quad w = -\cos(ky), \quad (6.9)$$

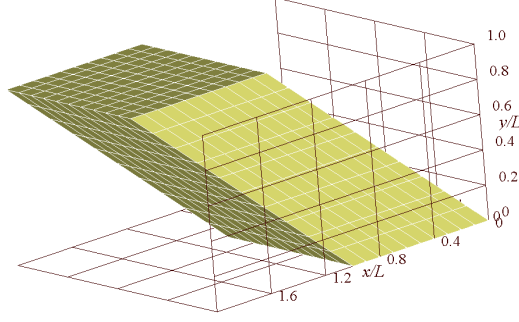
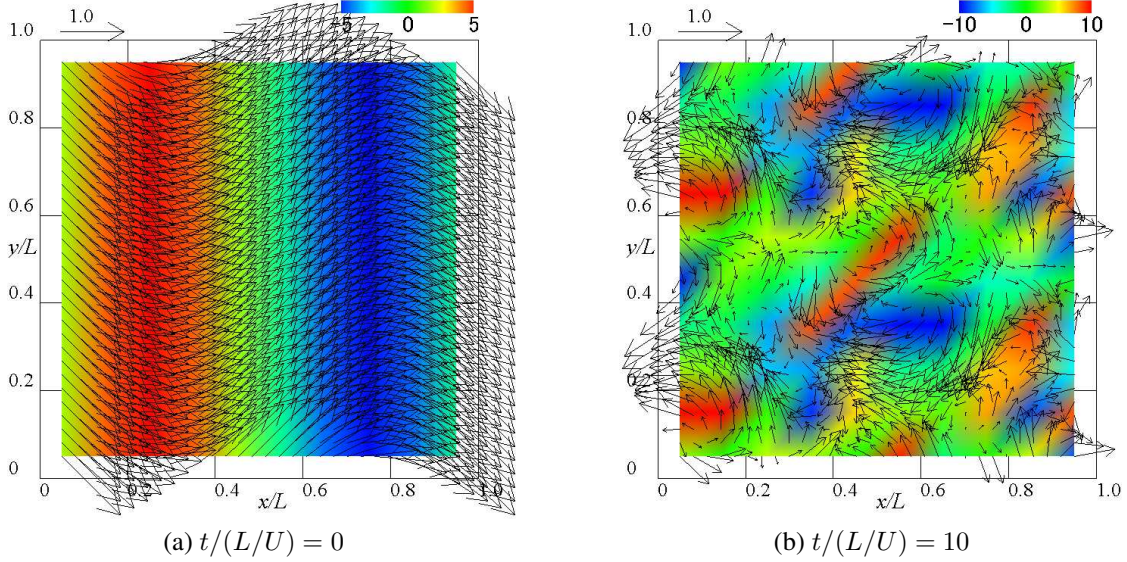


Figure 16: Skewed grid for a periodic inviscid flow


 Figure 17: Velocity vectors and vorticity contours at $z/L = 0.5$ for a periodic inviscid flow: $\Delta t/(L/U) = 0.01$

The expression (6.9) automatically satisfies the divergence-free condition $\nabla \cdot \mathbf{u} = 0$. Equation (6.9) is made dimensionless using the maximum velocity value U as a reference value.

The computational domain is a cube with a side of L . As for the initial condition, we give Eq. (6.8). Periodic boundary conditions are applied at all boundaries. This calculation uses a uniform grid of $N \times N \times N$. N is the number of grid points in each direction, and it was fixed at $N = 11$. To investigate the effect of grid non-orthogonality on calculation accuracy, we use the non-orthogonal grid shown in Fig. 16. The computational domain is tilted at an angle $\beta_1 = 45^\circ$ in the x -direction and an angle $\beta_2 = 60^\circ$ in the z -direction. A grid was generated as shown below:

$$y_{i,j,k} = \Delta y(j-1), \quad x_{i,j,k} = \Delta x(i-1) + \frac{y_{i,j,k}}{\tan(\beta_1)}, \quad z_{i,j,k} = \Delta z(i-1) + \frac{y_{i,j,k}}{\tan(\beta_2)}, \quad (6.10)$$

where Δx , Δy , and Δz are the grid widths in the x -, y -, and z -directions, respectively. As the reference values used in this calculation, $l_{\text{ref}} = L$ and $u_{\text{ref}} = U$. The time step is changed from $\Delta t/(L/U) = 0.0005$ to 0.1 , and we investigate the influence of the computational method on the time accuracy. The Courant number is defined as $\text{CFL} = \Delta t U / \Delta x$ and changes as $\text{CFL} = 0.005 - 1.0$ according to the time step. In this calculation, as an interpolation method of cell interface velocity, we use not only Rhie–Chow’s interpolation but also direct interpolation, which does not use weighted interpolation by pressure.

Figure 17 shows velocity vectors and z -direction vorticity contours in the x - y cross-section at times $t/(L/U) = 0$ and 10 . The result at $t/(L/U) = 10$ was obtained using this numerical method. Although the initial state is a periodic flow field with wavelength $\lambda/L = 1.0$, at $t/(L/U) = 10$, the turbulence of twice the wave number component occurs, and the flow field develops into an unsteady and turbulent flow. It is found that, unlike the Taylor damping vortex, the initial state is not maintained.

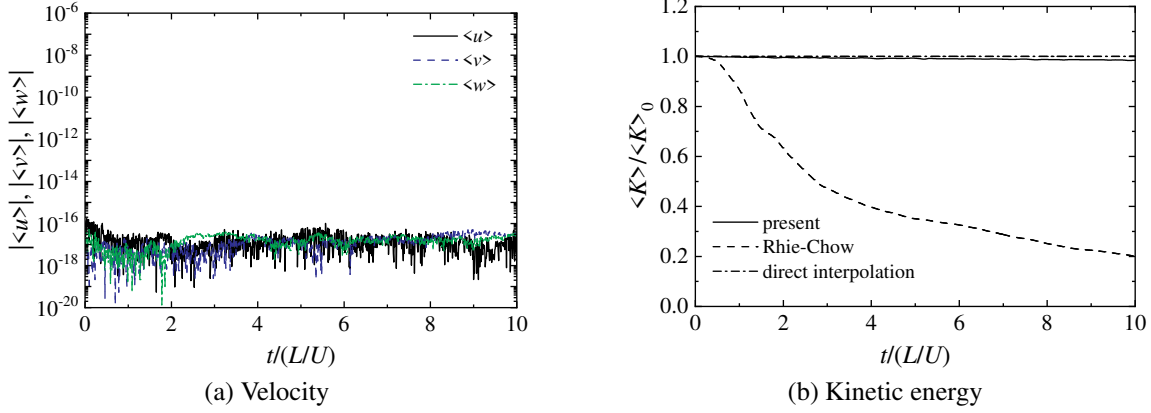


Figure 18: Total amounts of velocity and kinetic energy using orthogonal grid for a periodic inviscid flow: $\Delta t/(L/U) = 0.01$

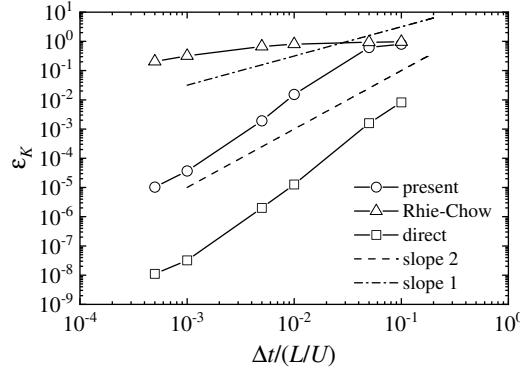


Figure 19: Kinetic energy error using orthogonal grid for a periodic inviscid flow

As this computational model is a periodic flow, the total amount of velocity is conserved for $Re = \infty$. First, we consider the results using the orthogonal grid. Figure 18(a) shows the total amount, $\langle u \rangle$, of velocity obtained using this numerical method. The total amounts for all velocity components change at low levels, indicating the excellent conservation of velocity. The total amount, $\langle K \rangle$, of kinetic energy is shown in Fig. 18(b). This calculated result almost agrees with that by direct interpolation, indicating that the energy is preserved. In the case of Rhie–Chow’s interpolation, we can see that $\langle K \rangle$ decays rapidly, and the energy is not conserved.

Figure 19 shows the relative error, $\varepsilon_K = |(\langle K \rangle - \langle K \rangle_0)/\langle K \rangle_0|$, of kinetic energy. Here, the subscript 0 represents the initial value. As the time step Δt decreases, the error ε_K in this numerical method decreases with a slope of 2, similar to the direct interpolation method, indicating second-order convergence. In the direct interpolation without weighted interpolation by pressure, the error is lower than in the present scheme, and the weighted interpolation by pressure difference in this numerical method increases the error. The Rhie–Chow interpolation gives the kinetic energy a first-order accuracy error to time. However, Rhie–Chow interpolation does not show linear convergence, and lowering Δt hardly reduces the error.

Next, we consider the results using the non-orthogonal grid. Figure 20(a) shows the total amount, $\langle u \rangle$, of velocity obtained using this computational method. As in the case of the orthogonal grid, the total amount is at the rounding error level, and the conservation of velocity is excellent. The total amount, $\langle K \rangle$, of kinetic energy is shown in Fig. 20(b). Compared with the results by direct interpolation, the total amount obtained by this calculation method decreases slightly with time, and the energy conservation deteriorates. The Rhie–Chow interpolation does not conserve the kinetic energy.

Figure 21 shows the relative error, $\varepsilon_K = |(\langle K \rangle - \langle K \rangle_0)/\langle K \rangle_0|$, of kinetic energy. Even with the non-orthogonal grid, the error is at the same level as with the orthogonal grid. No deterioration in calculation accuracy is observed, and the second-order accuracy is maintained.

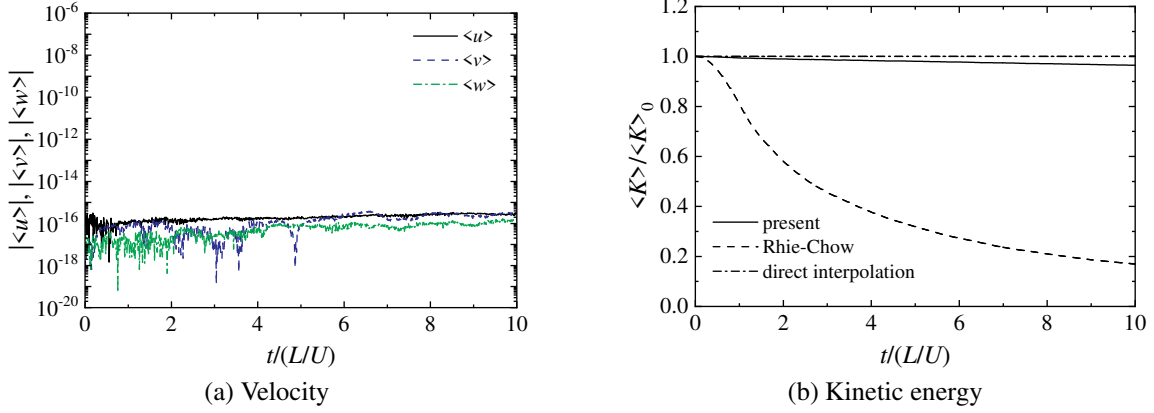


Figure 20: Total amounts of velocity and kinetic energy using skewed grid for a periodic inviscid flow: $\Delta t/(L/U) = 0.01$

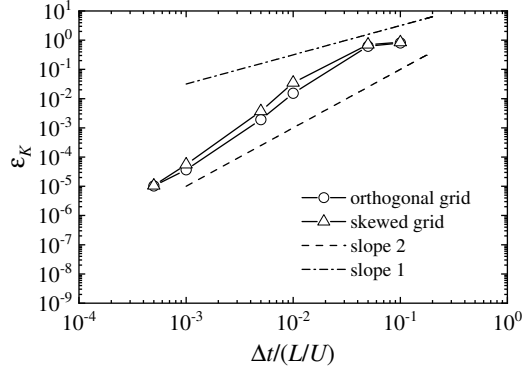


Figure 21: Kinetic energy errors using orthogonal and skewed grids for a periodic inviscid flow

In this analysis, we investigated the inviscid flow. Even when analyzing unsteady flows with high Reynolds numbers, the Rhie–Chow interpolation method is expected to cause a significant attenuation of kinetic energy. It is believed that the improved scheme constructed in this study is effective in suppressing the attenuation of kinetic energy.

7 Conclusion

This study constructed a finite difference scheme for incompressible fluids using a collocated grid in a general curvilinear coordinate system. The velocity at the cell interface is determined by weighted interpolation based on the pressure difference to prevent pressure oscillations. The Poisson equation for the pressure correction value is solved with the cross-derivative term omitted to improve calculation efficiency. In addition, simultaneous relaxation of velocity and pressure is applied to improve convergence. We analyzed steady flow fields to verify the validity of this numerical method. Even without the cross-derivative term, calculations could be stably performed, and convergent solutions were obtained. We investigated the conservation property of kinetic energy in unsteady flow fields and verified the accuracy of the cell interface interpolation method developed in this study. In inviscid flow, this computational method can suppress the attenuation of kinetic energy. In addition, it was revealed that the conservation of kinetic energy is excellent even with a non-orthogonal grid and that the calculation results have second-order accuracy to time, regardless of the grid. In the viscous analysis, when the Reynolds number increased, the error in this numerical method was lower than that of the Rhie–Chow interpolation method. It has been clarified that the present numerical scheme improves calculation accuracy in unsteady flows. In the future, we will apply this computational method to numerical analyses of coherent vortices and heat transport at high Reynolds number flows.

Acknowledgment

The numerical results in this research were obtained using supercomputing resources at the Cyberscience Center, Tohoku University. This research did not receive any specific grant from funding agencies in the public, commercial, or not-for-profit sectors. We would like to express our gratitude to Associate Professor Yosuke Suenaga of Iwate University for his support of our laboratory. The authors wish to acknowledge the time and effort of everyone involved in this study.

Author declarations

Conflicts of interest: The authors have no conflicts to disclose.

Author contributions: Hideki Yanaoka: Conceptualization (lead); Data curation (lead); Formal analysis (lead); Investigation (lead); Methodology (lead); Software (lead); Validation (lead); Visualization (lead); Writing – original draft (lead); Writing – review and editing (lead).

References

- Amsden, A.A., Harlow, F.H., 1970. A simplified MAC technique for incompressible fluid flow calculations. *J. Comput. Phys.* 6, 322–325. doi:doi:[https://doi.org/10.1016/0021-9991\(70\)90029-X](https://doi.org/10.1016/0021-9991(70)90029-X).
- Barakos, G., Mitsoulis, E., Assimacopoulos, D., 1994. Natural convection flow in a square cavity revisited: Laminar and turbulent models with wall functions. *Int. J. Numer. Methods Fluids* 18, 695–719. doi:doi:<https://doi.org/10.1002/fld.1650180705>.
- Bartholomewa, P., Dennera, F., Abdol-Azisa, M.H., Marquisa, A., G.M.van Wachema, B., 2018. Unified formulation of the momentum-weighted interpolation for collocated variable arrangements. *J. Comput. Phys.* 375, 177–208. doi:doi:<https://doi.org/10.1016/j.jcp.2018.08.030>.
- Choi, S.K., 1999. Note on the use of momentum interpolation method for unsteady flows. *Numer. Heat Tr. A-Appl.* 36, 545–550. doi:doi:<https://doi.org/10.1080/104077899274679>.
- De Vahl Davis, G., 1983. Natural convection of air in a square cavity: A bench mark numerical solution. *Int. J. Numer. Methods Fluids* 3, 249–264. doi:doi:<https://doi.org/10.1002/fld.1650030305>.
- Fuchs, L., Tillmark, N., 1985. Numerical and experimental study of driven flow in polar cavity. *Int. J. Numer. Methods Fluids* 5, 311–329. doi:doi:<https://doi.org/10.1002/fld.1650050403>.
- Harlow, F.H., Welch, J.E., 1965. Numerical calculation of time-dependent viscous incompressible flow of fluid with free surface. *Phys. Fluids* 8, 2182–2189. doi:doi:<https://doi.org/10.1063/1.1761178>.
- Hirt, C.W., Nichols, B.D., Romero, N.C., 1975. SOLA: A numerical solution algorithm for transient fluid flows. Technical Report LA-5852. Los Alamos Scientific Lab., N. Mex.(USA). doi:doi:<https://doi.org/10.2172/4205348>.
- Kim, J., Moin, P., 1985. Application of a fractional-step method to incompressible Navier–Stokes equations. *J. Comput. Phys.* 59, 308–323. doi:doi:[https://doi.org/10.1016/0021-9991\(85\)90148-2](https://doi.org/10.1016/0021-9991(85)90148-2).
- Lee, W., Jung, E., Kang, S., Hur, N., 2019. On a momentum interpolation scheme for collocated meshes with improved discrete kinetic energy conservation. *J. Mech. Sci. Technol.* 33, 2761–2768. doi:doi:<https://doi.org/10.1007/s12206-019-0522-8>.
- Majumdar, S., 1988. Role of underrelaxation in momentum interpolation for calculation of flow with nonstaggered grids. *Numer. Heat Tr.* 13, 125–132. doi:doi:<https://doi.org/10.1080/10407788808913607>.
- Morinishi, Y., 1998. Fully conservative higher order finite difference schemes for incompressible flow. *J. Comput. Phys.* 143, 90–124. doi:doi:<https://doi.org/10.1006/jcph.1998.5962>.
- Morinishi, Y., 1999. Improvement of collocated finite difference scheme with regard to kinetic energy conservation. *JSME, Ser. B* 65, 505–512. doi:doi:<https://doi.org/10.1299/kikaib.65.505>. (in Japanese).
- Patankar, S.V., Spalding, D.B., 1972. A calculation procedure for heat, mass and momentum transfer in three-dimensional parabolic flows. *Int. J. Heat Mass Transf.* 15, 1787–1806. doi:doi:[https://doi.org/10.1016/0017-9310\(72\)90054-3](https://doi.org/10.1016/0017-9310(72)90054-3).
- Perić, M., 1990. Analysis of pressure-velocity coupling on nonorthogonal grids. *Numer. Heat Tr. B-Fund.* 17, 63–82. doi:doi:<https://doi.org/10.1080/10407799008961733>.
- Perić, M., Kessler, R., Scheuerer, G., 1988. Comparison of finite-volume numerical methods with staggered and collocated grids. *Comput. Fluids* 16, 389–403. doi:doi:[https://doi.org/10.1016/0045-7930\(88\)90024-2](https://doi.org/10.1016/0045-7930(88)90024-2).

- Rhie, C.M., Chow, W.L., 1983. Numerical study of the turbulent flow past an airfoil with trailing edge separation. *AIAA J.* 21, 1525–1532. doi:doi:<https://doi.org/10.2514/3.8284>.
- Rosenfeld, M., Kwak, D., Vinokur, M., 1991. A fractional step solution method for the unsteady incompressible Navier–Stokes equations in generalized coordinate systems. *J. Comput. Phys.* 94, 102–137. doi:doi:[https://doi.org/10.1016/0021-9991\(91\)90139-C](https://doi.org/10.1016/0021-9991(91)90139-C).
- Takemitsu, N., 1985. Finite difference method to solve incompressible fluid flow. *J. Comput. Phys.* 61, 499–518. doi:doi:[https://doi.org/10.1016/0021-9991\(85\)90077-4](https://doi.org/10.1016/0021-9991(85)90077-4).
- Taylor, G.I., 1923. Lxxv. on the decay of vortices in a viscous fluid. *The London, Edinburgh, and Dublin Philosophical Magazine and Journal of Science, Series 6* 46, 671–674. doi:doi:<https://doi.org/10.1080/14786442308634295>.
- Van der Vorst, H.A., 1992. Bi-CGSTAB: A fast and smoothly converging variant of Bi-CG for the solution of non-symmetric linear systems. *SIAM J. Sci. and Stat. Comput.* 13, 631–644. doi:doi:<https://doi.org/10.1137/0913035>.
- Van Doormaal, J.P., Raithby, G.D., 1984. Enhancements of the SIMPLE method for predicting incompressible fluid flows. *Numer. Heat Tr.* 7, 147–163. doi:doi:<https://doi.org/10.1080/01495728408961817>.
- Wu, X., Squires, K.D., Wang, Q., 1995. Extension of the fractional step method to general curvilinear coordinate systems. *Numer. Heat Tr. B- Fund.* 27, 175–194. doi:doi:<https://doi.org/10.1080/10407799508914952>.
- Yanaoka, H., 2023. Influences of conservative and non-conservative Lorentz forces on energy conservation properties for incompressible magnetohydrodynamic flows. *J. Comput. Phys.* 491, 112372 (36 pages). doi:doi:<https://doi.org/10.1016/j.jcp.2023.112372>.
- Yanaoka, H., Inafune, R., 2023. Frequency response of three-dimensional natural convection of nanofluids under microgravity environments with gravity modulation. *Numer. Heat Tr. A-Appl.* 83, 745–769. doi:doi:<https://doi.org/10.1080/10407782.2022.2161437>.
- Yu, B., Kawaguchi, Y., Tao, W.Q., Ozoe, H., 2002. Checkerboard pressure predictions due to the underrelaxation factor and time step size for a nonstaggered grid with momentum interpolation method. *Numer. Heat Tr. B- Fund.* 41, 85–94. doi:doi:<https://doi.org/10.1080/104077902753385027>.
- Zang, Y., Street, R.L., Koseff, J.R., 1994. A non-staggered grid, fractional step method for time-dependent incompressible Navier–Stokes equations in curvilinear coordinates. *J. Comput. Phys.* 114, 18–33. doi:doi:<https://doi.org/10.1006/jcph.1994.1146>.